SEARCH FOR MIDDLE ATMOSPHERE WAVES OVER ARECIBO: LIDAR OBSERVATIONS AND ANALYSIS TECHNIQUES

by

Giovanni Astacio Oquendo

A project report submitted in partial fulfillment of the requirements for the degree of

MASTER OF ENGINEERING
in
ELECTRICAL ENGINEERING

UNIVERSITY OF PUERTO RICO
MAYAGÜEZ CAMPUS
2012

Approved by:

______________________________ __________________
Henrick M. Ierkic, PhD — Date
President, Graduate Committee

______________________________ __________________
Nayda G. Santiago, PhD — Date
Member, Graduate Committee

______________________________ __________________
José M. Rosado, PhD — Date
Member, Graduate Committee

______________________________ __________________
Kurt Allen Grove, PhD — Date
Representative of Graduates Studies

______________________________ __________________
Pedro I. Rivera, PhD — Date
Chairperson of the Department

Abstract of Dissertation Presented to the Graduate School of the University of Puerto Rico in Partial Fulfillment of the Requirements for the Degree of Master in Electrical Engineering

SEARCH FOR MIDDLE ATMOSPHERE WAVES OVER ARECIBO: LIDAR OBSERVATIONS AND ANALYSIS TECHNIQUES

By
Giovanni Astacio Oquendo
May 2012

Chair: Henrick M. Ierkic
Major Department: Electrical and Computer Engineering

This work presents a set of different processing techniques to analyze Lidar observations in order to search for middle atmosphere waves over Arecibo $\left(18^{\circ}21'N, 66^{\circ}45'W\right)$. The processing analysis includes algorithms to detect sampling continuity, data gaps, and outliers in the observations. Also, we can observe time sequences for vertical profiles, bi-dimensional images, and vertical perturbations. Standard deviations from the mean temperature profile are shown using error bars. A standard model, MSIS-90, that presents the neutral temperature and densities of the middle atmosphere was used to compare with the obtained results.

The analysis used data from two Lidar campaigns of three consecutive days each. The observed wavelengths were 355 nm and 532 nm. The data was analyzed statistically and an algorithm to search for waves using a periodogram was developed. The presentation of the results was organized using standard meteorological styles.

Resumen de Disertación Presentado a Escuela Graduada de la Universidad de Puerto Rico
Como Requisito Parcial de los Requerimientos para el Grado de Maestría en Ingeniería Eléctrica

BUSQUEDA DE ONDAS EN LA ATMOSFERA MEDIA SOBRE ARECIBO: OBSERVACIONES DE LIDAR Y TECNICAS DE ANALISIS

Por
Giovanni Astacio Oquendo
May 2012

Consejero: Henrick M. Ierkic
Departamento: Ingeniería Eléctrica y Computadoras

Este trabajo presenta un conjunto de diferentes técnicas de procesamiento para analizar observaciones de Lidar con el propósito de encontrar ondas en la atmósfera media sobre Arecibo (18°21’N,66°45’W). El procesamiento incluye algoritmos para detectar continuidad del muestreo, huecos y puntos extremos en las observaciones. Además, incluye secuencias de tiempo de perfiles verticales, imágenes bi-dimensionales y perturbaciones verticales. La desviación estandar sobre el promedio del perfil vertical de temperatura se muestra mediante barras de error. Para comparar los datos obtenidos, se utilizó el modelo MSIS-90, que presenta las temperaturas neutrales y densidades en la atmósfera media.

El análisis fue basado en dos campañas de observación de Lidar de tres días consecutivos cada una. Se utilizaron largos de onda de observación de 355nm y 532nm. Los datos fueron analizados estadísticamente, y se desarrolló un algoritmo para encontrar periodicidades de onda utilizando periodogramas. La presentación de los resultados fue organizada utilizando estilos estándares del área meteorológica.

To GOD…

To my family…

ACKNOWLEDGEMENTS

I would like to start by giving thanks to GOD. I recognize that this work was possible due to His support. I have matured, both, as a professional, and as a human being thanks to my experiences in the different areas acquired during this endeavor. During the last two years at UPRM, I had the opportunity to meet new people that took part in my development.

I thank, Dr. Henrick M. Ierkic who served as my advisor and a liaison with the Arecibo Observatory. The dedicated hours of meetings, guiding and mentoring my work, were a valuable base to complete this project. We dedicated numerous meetings in which he explained many theories. The MatLab codes were developed in a common effort.

I thank Dr. Nayda G. Santiago, for serving as a member of my graduate committee. She helped and advised in the process to find my advisor. She provided me with different educational materials that served as an important guide for my work.

Thanks to another member of my graduate committee, Dr. José M. Rosado. We shared excellent advising conversations related to my project. He, also, gave me advice on how to pursue life-long learning with my research.

When I needed the three members of my graduate committee, they were always present. Thanks to Dr. Kurt Allen Grove, graduate studies representative, for his valuable recommendations to my work in coordination with my graduate committee.

Special thanks for the Optical Science Group of the Arecibo Observatory. Dr. Shikha Raizada provided the data used in this project. She explained the general characterization of the Lidar theory. She took us on tours of the Optical Laboratory at Arecibo. Thanks to Dr.

Craig Tepley for recommendations about our results. Thanks to Dr. Sumanta Sarkhel, for sharing the unevenly spaced data code.

Thanks to the professors, that taught me the courses at graduate level. I also give my gratitude to Mrs. Sandra Montalvo for her counseling. I thank the Dean of Students, Dr. Victor Siverio, for his help at the beginning of my graduate studies. Thanks to my classmates for their friendship. I am whole-heartedly thankful to my mother María, my family, and friends for believing in me, and always being there for me.

Table of Contents

Table List

Figure List

1 Introduction

Middle atmosphere dynamics are influenced by the troposphere, which acts as a sink for many stratospheric constituents (N_2, O_2 y Ar) and as a source of wave generation [Devie et al., 2002]. The waves in this region influence the density and temperature. Gravity waves play an important role in the middle atmosphere wind and temperature field variability [Murthy 1998 in Gurahay, 2008]. Studies related to middle atmosphere dynamics have expanded as the coupling between the stratospheric changes and the low level climate is searched for [Nappo, 2002].

The scientific community has been conducting middle atmosphere studies recognizing the importance of gravity waves in the determination of the gross circulation through the process of momentum deposition. Another concern is with the global temperature, and what changes in the standard temperature profiles affect atmospheric stratification. The Earth's atmosphere is a system characterized by processes that may vary [Mackenzie, 1998]. We can observe changes in this system, or how equilibrium conditions are established. Problems arise when environmental change induced by natural process is influence by human activities. Anthropogenic contamination has been influencing atmosphere since the beginning of the industrial revolution [Lastovicka, et al., 2010].

The means for determining variability in the Earth system requires observation of shifts about some mean relative point. In this sense we need to create standard observations of the processes, which complement the background studies. This is the first statement that justifies our work, the requirement of data that characterize the meteorological system, specifically, the middle atmosphere behavior.

The objective of this study was to identify and characterize waves in the middle atmosphere using statistical signal analysis on the Lidar observations. To achieve this, we present a step-by-step description of the process, from receiving the raw data to identifying signal.

We conducted exploratory statistical analysis in order to obtain *A Priori* characteristics of the raw data**.** We then processed the data with the standard spectral analysis using the fast Fourier transforms (FFT) algorithm, in order to detect waves in noisy data and apply a statistical test to find the intensity of wave periodicities. We use the Fisher test to analyze detection fidelity and MatLab software for FFT analysis. Amplitude and phase profiles characterize the potential energy density, and were used to determine the vertical wavelength of gravity waves. An alternate version of the analysis was needed for the spectral analysis of unevenly sampled raw data. We compared the results for both spectral analyses in order to describe the effectiveness of each technique. To obtain equal results, we had to treat the unevenly distributed raw data to eliminate gaps, and then apply the regular Fourier analysis. We contrasted how the activity differs with altitude, and date. The deviation between the MSIS-90 model and Lidar model was also evaluated.

1.1 Objectives and Problem Statement

The goal of this project is to identify a set of different processing techniques to analyze Lidar observations in order to search for middle atmosphere waves. We want to detect sampling continuity, data gaps, and outliers to decide how apply a spectral analysis with the purpose to obtain the frequency behavior of time series. Reusable codes for the process of data analysis performing a compendium of the analysis techniques used to search for middle atmosphere waves are needed.

The maintenance and propagation of wave motion is a characteristic of a stably stratified fluid like the atmosphere except where the planetary boundary layer combines convection with wind shear producing mixing through the troposphere [Nappo, 2002]. With stable stratification, we can assume the presence of gravity waves in the atmosphere. A wide range of wave frequencies may be present, lasting from a few minutes to hours. Waves are observed ascending or descending with time and appear or disappear intermittently [Nappo, 2002]. It is important to emphasize that Nappo (2002) indicates that the gravity waves in the middle atmosphere appear to be nearly monochromatic. This observation was tested with a spectral analysis in order to find waves of a single periodicity. This theoretical observation is the principal hypothesis we wish to test.

LIDAR technology and other scientific remote sensing observation tools were compared using series of experiments to characterize the patterns in the middle atmosphere. This requires an analysis of observed data compared with the standard theoretical models.

Waves periodicities are difficult to identify in the bi-dimensional image shown in Figures 1 – 6, and or in the raw data time series (Figures 16 – 27). We applied a statistical signal analysis in order to find gravity waves in the two-campaign temperature observations. Refer to Table 2 for the data of the campaigns. The bi-dimensional images, Figures 1 - 6, are the results of the subtraction of the mean vertical profile from each time observations of the vertical temperature profile. The bi-dimensional images of Figures 1 - 6 present the perturbations for the two data campaigns.

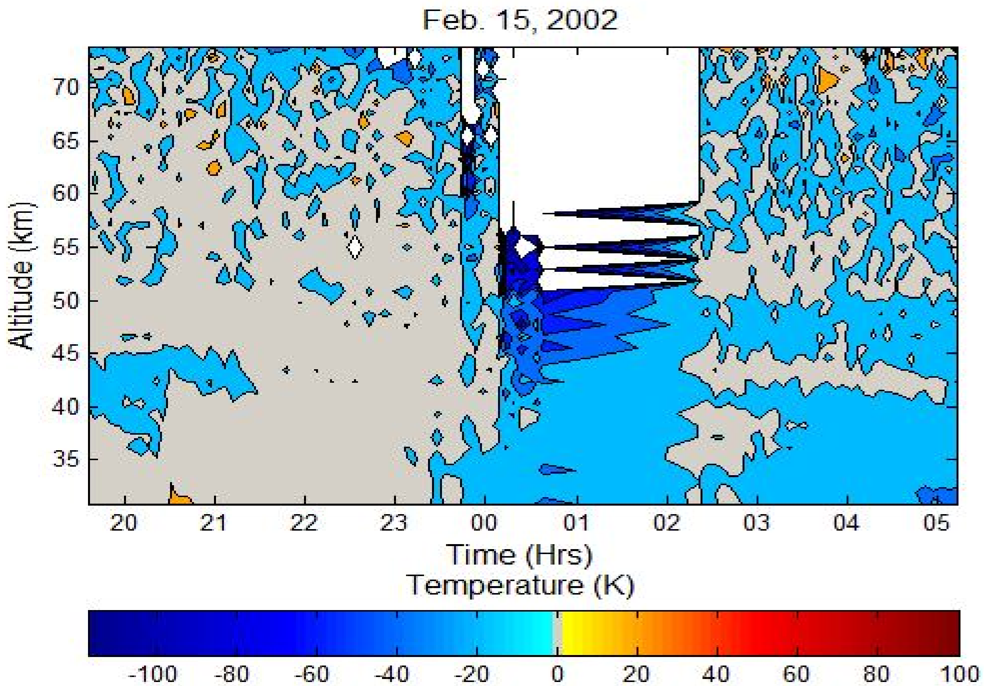

Figure 1: Temperature perturbations for February 15, 2002

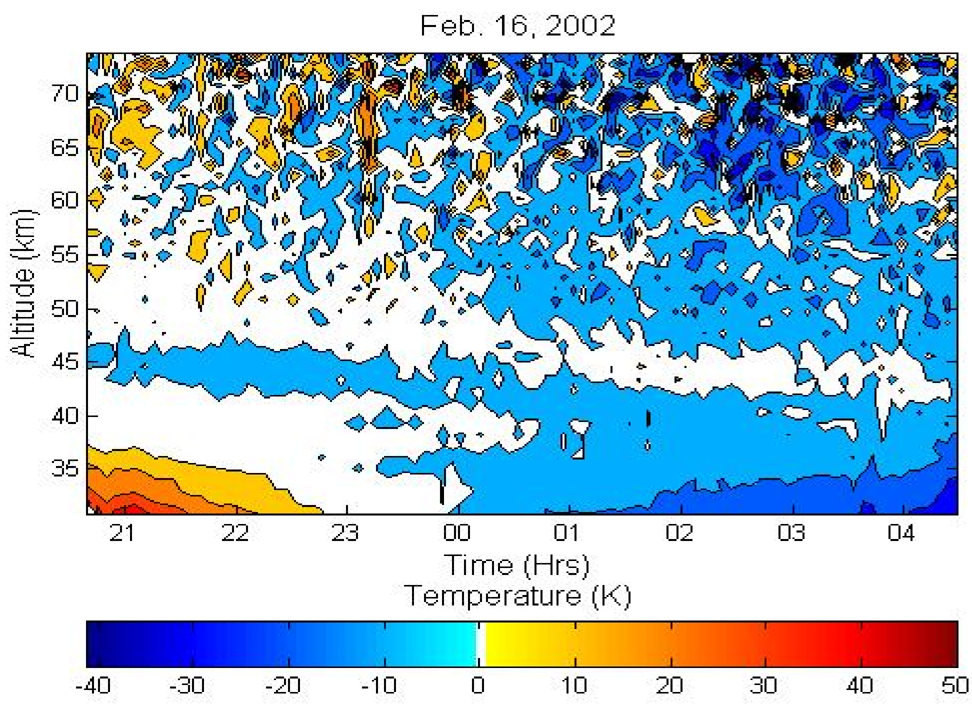

Figure 2: Temperature perturbations for February 16, 2002

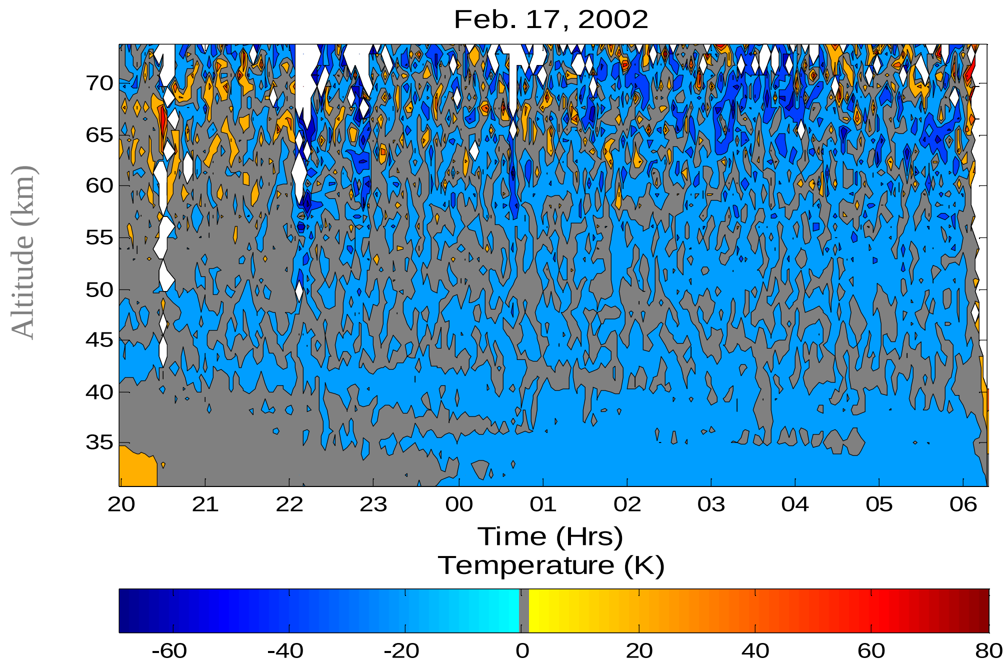

Figure 3: Temperature perturbations for February 17, 2002

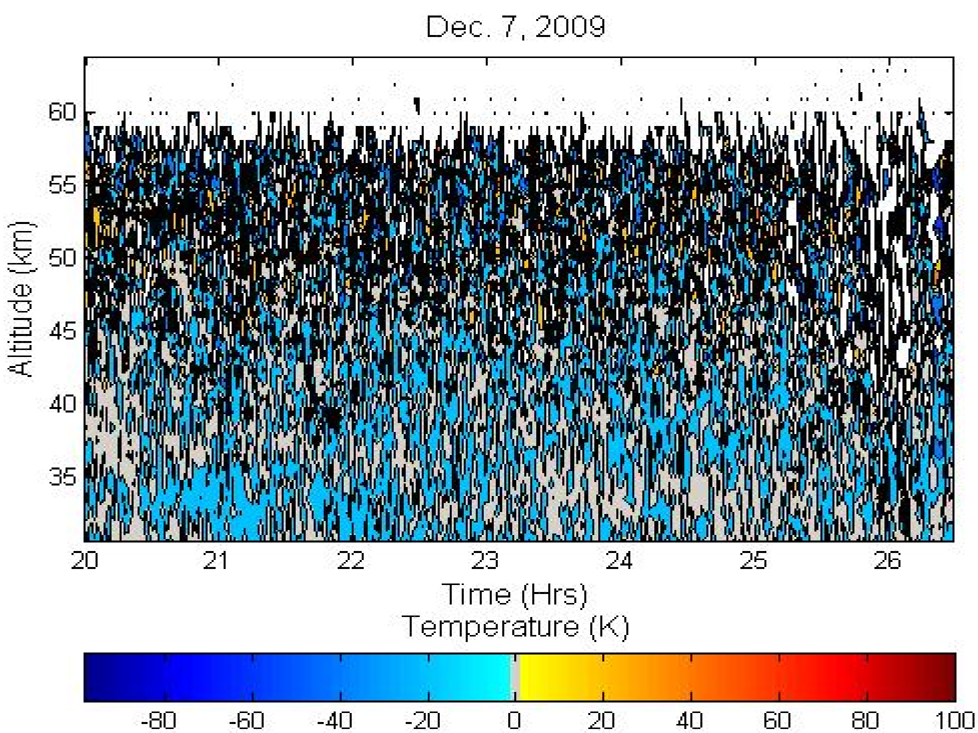

Figure 4: Temperature perturbations for December 7, 2009

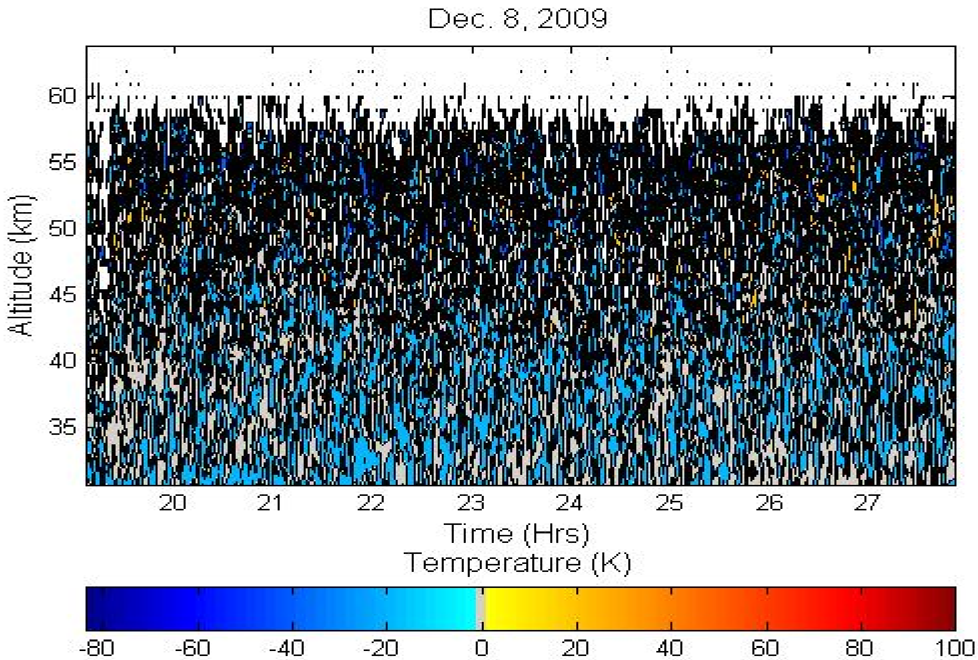

Figure 5: Temperature perturbations for December 8, 2009

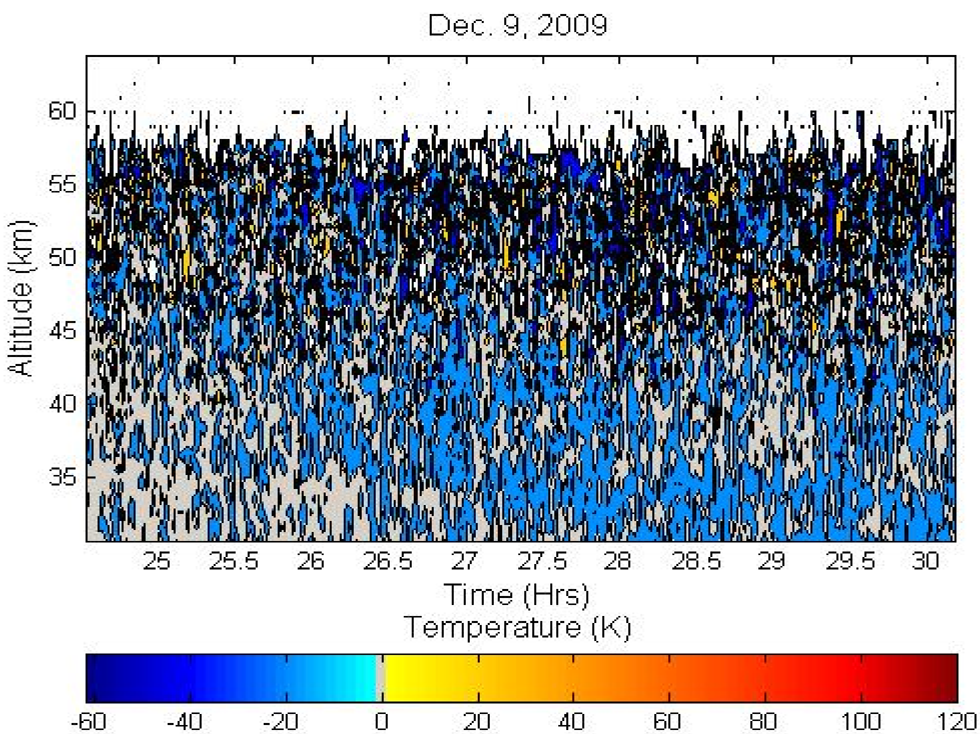

Figure 6: Temperature perturbations for December 9, 2009

We observe in Figures 1 - 6 the temperature perturbations for approximately 4 - 10 hours of data. We can better appreciate the vertical perturbation when we subtract of a third order polynomial fit from the vertical mean temperature profile discussed below.

There are several publications that describe the processing of the signal observations obtained by Lidar for the purpose of identifying wave periodicities in the middle atmosphere, and the affect the temperature profile. For the tropical region, the contributions to database and analysis are few. We need more results that present the processing of the middle atmosphere data from Puerto Rico in order to identify gravity waves. Another needed contribution will came from comparisons between the standard temperature vertical profiles, gathered by other remote sensing instruments, with the greater sensitivity of Lidar data. We were applying statistical signal processing techniques using appropriate methods that consider the problem of noise.

1.2 Literature Review

A revision of literature is being conducted as a part of the project. First, we want to understand the Lidar system and data acquisition. The Optical Science Group of the Arecibo Observatory has provided temperature profiles obtained from observed density data. The process to obtain temperature from Lidar observation is explained by Hauchecorne et al. (1980). Hines (1960) carried out the first theoretical study of gravity waves on the middle atmosphere dynamics [Guharay et al. 2008]. Fritts (1984) presents a study of the middle atmosphere characterization. We used Hui et al. (2012) to explain the layers of the atmosphere. The scattering process was analyzed for this project using the method from Measures (1992), and Weitkamp (2005).

1.3 Project Outline

This work is organized as follows:

- In Chapter 2 we observe a theoretical background that includes the description of the atmosphere and the models that characterizes it behavior. In addition, a general description of the Lidar system and the techniques of operation of the backscattering theory are discussed. The experimental implementation is discussed in this chapter.
- In order to presents the analysis of the data we observe a description for the sampling methodology used to analyze the data in Chapter 3. A standard model of temperature is described in addition to the Lidar model. A set of processing techniques was created to characterize the data in order to support the spectral analysis.
- In Chapter 4 we presents the conclusions and the recommendations for future work.

2 Theoretical Background

In order to have the better understanding about the character of the Lidar observations in the middle atmosphere, and how characteristics to analyze it, we discuss the theoretical background.

2.1 Middle Atmosphere Characterization

The middle atmosphere is the region of the atmosphere from 12 to 80 km. This region contains the stratosphere and mesosphere. Several dynamic processes characterize the middle atmosphere. The troposphere acts as a sink for many atmospheric gases (N_2, O_2, and Ar), and a place where wave activity complicates the dynamics of the middle atmosphere. The temperature and density structures in this region are considered influenced by these waves [Fritts, 1984].

Using the change in temperature with the increasing altitude, we see the structured layers in the atmosphere of the Earth. A description of the vertical temperature profile has been presented by Hui et al. (2012). Figure 7 summarizes a description of the bottom four layers of the atmosphere [Strobel, copyright 1998 - 2011].

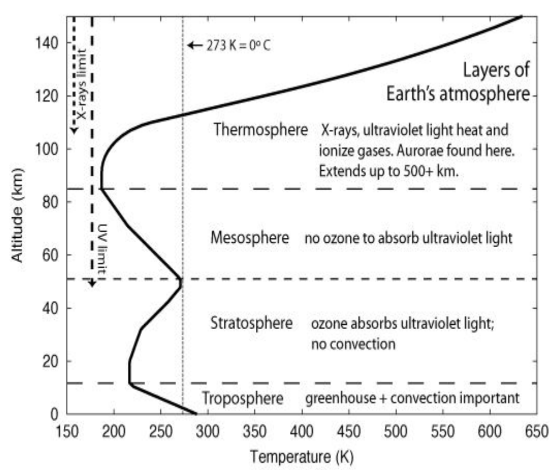

Figure 7: Bottom four layers of the Earth's atmosphere
Nick Strobel (1998 - 2011) **http://www.astronomynotes.com/copyright.htm**

The troposphere is the layer closets to the surface of the earth, and extends up to 10 – 15 km. The temperature and pressure drops increasing the altitude in this region. At the top of troposphere is the tropopause, which is the point where rising water vapor cannot go higher. This effect stands out because the vapor changes into ice and is trapped. These clouds and other weather conspicuous phenomena operate in the troposphere due to this trap. One of these phenomena is the Greenhouse effect, where the heat of the Sun warms the surface of the Earth and most of this heat is sent back to the space by radiation. Water vapor and carbon dioxide trap some of this heat and the trapping of heat is called the Greenhouse effect. Today, the increase of carbon dioxide is being blamed for global warming.

The stratosphere extends 15 to 50 km above the earth surface. A nearly constant temperature with altitude characterizes the lower portion of the stratosphere. The capture of sunlight by ozone, which absorbs most of the harmful ultraviolet rays of the Sun, fun increases the temperature in the upper portion of the stratosphere.

The mesosphere extends from an altitude of 50 to 80 km. This is a cold layer characterized by a decreasing temperature with the increasing altitude. The thermosphere extends from 80 km above and is characterized by hot temperature.

2.2 Lidar System

Lidar is an acronym for Light Detection and Ranging. The optical team of the Arecibo Observatory uses Hauchecorne et al. (1980) as reference work. This Lidar system is used to obtain the density and temperature profile between 35 and 70 km. Their Lidar is shown in the

Figure 8. It consists of a laser used as a transmitter, and of a telescope, which receives the backscattered photons from the atmosphere.

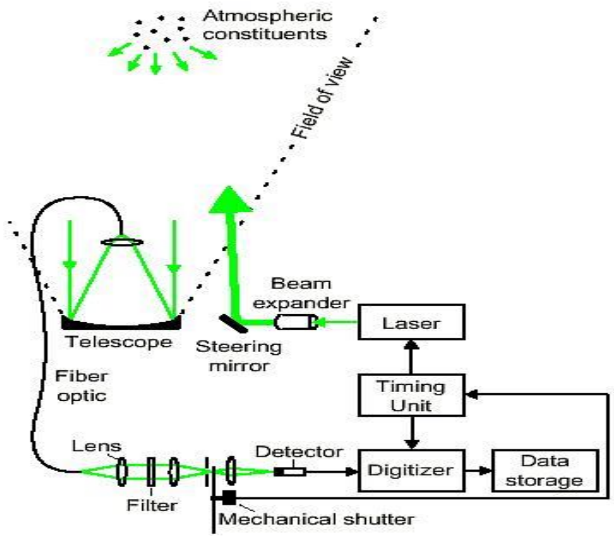

Figure 8: Basic Lidar System
Courtesy of Dr. Shikha Raizada (Arecibo Observatory)

Radar and Lidar are the predominant remote sensing devices used to study the middle atmosphere. Various reasons justify the use of a Lidar to conduct the desired measurements. First, the monochromatic wave is less prevalent in radar data than in Lidar profiles [Miller et al., 1987]. Even more, Radar is not capable of monitoring the height concerning to our study. For this reason the studies wave activity has been conducted with Lidar. Unfortunately, clouds block Lidar and only sporadic time series segments have been recorded for experimental campaigns.

It is important to understand that a Lidar operates in the same way as Radar. The main difference is in the radiation wavelength. Lidar uses the light in the form of photons, while radar operates in the radio bands. For remote sensing of the Earth's atmosphere with a Lidar, the wavelengths used are from UV (ultraviolet) 10 – 100 nm, to NIR (near infrared) 1 – 10 μm, depending on the types of measurements being made.

2.2.1 System Observation Techniques

Lidar measurements can be based on various atmospheric scattering processes, which is divided in two types: the inelastic and the elastic backscatter [Measures, 1992]. In the inelastic, Raman scattering, we observe a change in frequency. This is a characteristic of the molecule from which the laser radiation is scattered. Figure 9 presents a schematic and physical description of inelastic scattering.

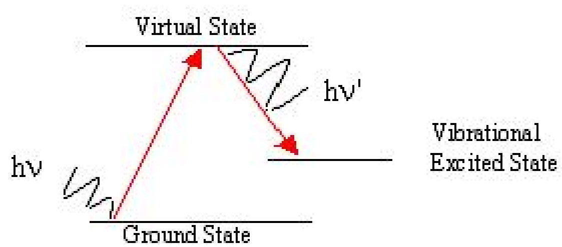

Figure 9: Raman Scattering
Modified of [Measures, 1992]

The characteristic frequency of the molecule $\Delta\upsilon$ is obtained by:

$$\upsilon' = \upsilon \pm \Delta\upsilon \,. \quad (2.1)$$

Two processes contribute a backscattered inelastic signal when a monochromatic wavelength is sent in the atmosphere [Hauchecorne et al., 1980]. These are the Rayleigh scattering by atmospheric molecules, and Mie scattering by atmospheric aerosols. Measurements for trace gases in the lower atmosphere use inelastic scattering. Raman scattering is understood as an inelastic scattering process, which involves the change of the energetic state of the molecule [Weitkamp, 2005].

Elastic-backscatter Lidar is the classic form of Lidar [Witkamp, 2005]. In elastic scattering we observe no change in frequency. The process in which the wavelength of the radiation remains unchanged is presented by elastic scattering examples of this type of scattering are: Rayleigh, Mie, and Resonance. The Figure 10 presents the Rayleigh and Mie scattering in particles. Rayleigh scattering is related to atomic and molecular scattering, while Mie scattering deals with aerosols where the particle size is comparable to wavelength. We consider nitrogen and oxygen as the source of Rayleigh- scattered radiation because about 99% of the Earth's molecular atmosphere is making up by these two gases [Weitkamp, 2005]. Resonance occurs deals when the laser wavelength is matched to the atomic transition frequency. The Rayleigh scattering intensity is proportional to λ^{-4}.

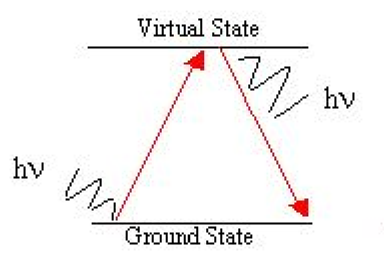

Figure 10: Rayleigh and Mie Scattering (Particles)
Modified of [Measures, 1992]

The Rayleigh scattering of the sunlight in the clear atmosphere is the reason of the blue color in the sky. The Rayleigh scattering creates diffuse scattering of incident solar radiation. Air scatters short λ light more than long λ light. Since blues are short λ the sky is blue in color. Figure 11 show the atmospheric regions where the Rayleigh and Raman techniques are used.

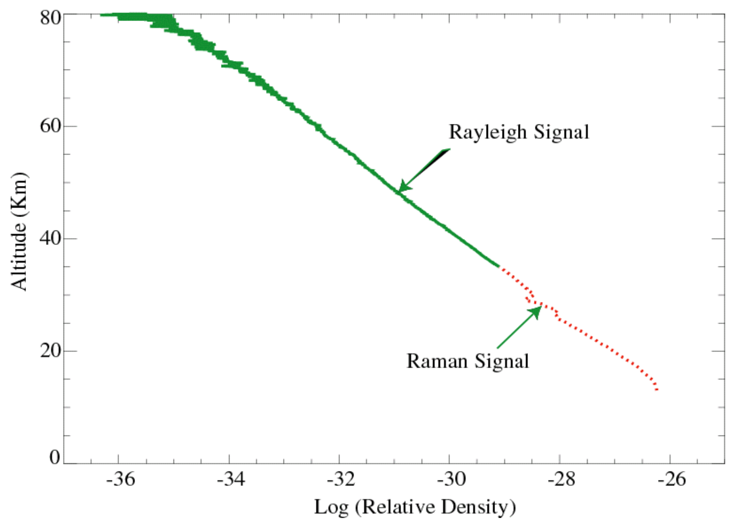

Figure 11: Example illustrating normalization of Rayleigh and Raman signal

2.2.2 System Description

The transmitter is the active part of the Lidar. This is a pulse laser, which has a high average power. The laser used is the Nd^{+++} or Yag laser. The receiver is a light collector. For good optical quality is necessary $-\frac{\lambda}{4}$ in the telescope. With a large telescope, we obtain better accuracy, but with higher cost. Laser technology compensates the cost of improving the telescope length. Table 1 presents the basic Lidar characteristics.

Table 1: Lidar characteristics

LIDAR CHARACTERISTICS	
LASER	
Type	Nd:Yag
Energy per Pulse	400mj at 532nm
	150mj at 355nm
Repetition Rate	10Hz
Pulse width	15ns
Divergence	4.10^{-4} rad
	10^{-4} rad (with a beam expander)
RECEIVER	
Telescope diameter	80 cm
Telescope area	0.5 m^2
Field of view	10^{-3} to 10^{-4} rad
Band pass filter	0.8 nm (FWHH)
P.F. interferometer	20 pm (FWHH)
Gate width	4um (0.6 km)

The wavelengths used with the data presented in this project from the Lidar of Arecibo are 532nm for the first campaign of observation, and 355nm for the second. Refer to Table 1 for the test specifications. The first one received measures until approximately 72 km, while the second recorded to an altitude approximately 65 km.

The data used in this project were obtained at the Arecibo Observatory located at 18°21'N, 66°45'W. The optical laboratory is located 350m northwest of the 305m radar reflector at an altitude of 363m [Beatty et al., 1992]. The observations offer measures of densities between 30km and 72km in the atmosphere. More specifically, the data measurements are from a Rayleigh Lidar operated at night. An inversion process that starts with the density profile was applied in order to obtain the temperature profile. This computation assumes that the atmosphere obeys the perfect gas law. A second assumption is the hydrostatic equilibrium of the atmosphere. The inversion method follows the description of Hauchecorne et al. (1980). Our observations were for three consecutive days in February 2002, and three consecutively days in December 2009. The data are summarized in the next Table 2.

Table 2: Campaign days and references files names

CAMPAIGN DATA 1&2	AO FILE NAME
2/15/2002	R2002046temp
2/16/2002	R2002047temp
2/17/2002	R2002048temp
12/7/2009	I09341_2min
12/8/2009	I09342_2min
12/9/2009	I09343_2min

2.3 Experimental Method Description

We obtained the data for two campaigns of observations from the Lidar of Arecibo Observatory. The data was obtained as temperature profile estimation. We did not participate in the inversion process to estimates the temperature from the densities obtained by the Lidar. In general, the Lidar technique consists of sending a vertically monochromatic laser pulse into atmosphere. The information about the structure and the composition of the atmosphere as a function of the altitude is provided by temporal analysis of the backscattered signal from air molecules and aerosols [Hauchercorne, 1980]. The first backscatter is from Rayleigh scattering, and a second from Mie scattering.

The following breakdown of equations used to estimate temperature from the observed photon intensity was obtained using Hauchercorne et al., (1980) reference. In the model used to estimate temperature from the atmosphere as a function of density to temperature, Hauchecorn et al. (1980) indicate that the altitude range of the measures is divided by the height range of the collection gate into n layers of thickness ΔZ. Using the measurement of density, the temperature is deduced, assuming that the atmosphere is in hydrostatic equilibrium and obeys the perfect gas law [Hauchecorne et al., 1980]. In the i^{th} altitude layer ($Z_i - \frac{\Delta z}{2}$, $z_i + \frac{\Delta z}{2}$), measured backscatter is:

$$N(z_i) = \frac{N_0 AKR_q T^2(z_0, z_i)}{4\pi(z_i - z_0)} \left| n_r(z_i)\beta_r + n_m(z_i)\beta_m \right| \Delta z \tag{2.2}$$

This equation assumes that the backscattered light is only due to Rayleigh and Mie scattering. In this equation the parameters are describe by Hauchecorne et al., 1980 as:

- $N(z_i)$ is the number of detected photons for one laser pulse and from a layer of thickness Δz centered at the height z_i.
- N_0 is the number of photons emitted for each laser pulse.
- The telescope area is A.
- The optical efficiency of the Lidar system is K, including the optical transmission through the transmitter and receiver.
- The quantum efficiency of the photo multiplier is R_q.

- The atmospheric transmission between the altitude of the Lidar site and the height of the emitting layer z_i is $T(z_0,z_i)$.
- The air molecules and aerosols concentrations are $n_r(z_i)$, and $n_m(z_i)$.
- The Rayleigh and Mie backscattering cross-sections are β_r and β_m.

When the Mie contribution is negligible at the altitude range between 35 an 80 km, the atmospheric density is given by the expression:

$$\rho(z) = \frac{C\left[S_L(z) - B(z)\right]}{T^2(z,\infty)} \tag{2.3}$$

- The signal coming from the altitude z, in a constant solid angle multiplied by $(z-z_0)^2$ and eventually corrected for non-linearity of the photo multiplier if this one is close to saturation is $S_{L(z)}$.
- The background signal due to dark current and sky background, extrapolated linearly for the altitude z is B(z).
- The atmospheric transmission between z and the top of the atmosphere, evaluated at the laser wavelength, taking into account ozone and Rayleigh attenuation is $T(z,\infty)$.
- A normalization constant, depends upon N_0, K, R_q, and $T(z_0,z_i)$ as defined above and may vary with time is C.

The measured C for each period is evaluated by fitting the density measured either with a standard model between 30 and 35 km, as MSIS-90 model. The relative uncertainty on the density determination is given by:

$$\frac{\Delta\rho}{\rho} = \frac{\Delta S_L(z)}{S_L(z) - B(z)}. \tag{2.4}$$

To determine the temperature, the assumption that the atmosphere is in hydrostatic equilibrium implies that the atmospheric turbulence does not affect the mean air density. The constant value for M for the air mean molecular weight is justified by the constant mixing ratio of the major atmospheric constituents (N_2, O_2, and Ar), and the negligible value of H_2O mixing ratio. The air pressure P(z), density $\rho(z)$, and the temperature T(z) are then related by:

$$P(z) = \frac{R\rho(z)T(z)}{M} \tag{2.5}$$

$$dP(z) = -\rho(z)g(z)dz \tag{2.6}$$

- The universal gas constant is R,
- The acceleration of gravity is g(z).

Combining the previous equations (2.5) and (2.6), we obtain:

$$\frac{dP(z)}{P(z)} = -\frac{Mg(z)}{RT(z)}dz = d(LogP(z)) \tag{2.7}$$

Assuming that the acceleration of gravity and the temperature are constant in the i^{th} layer, the pressure at the bottom and top of the layer are related by:

$$\frac{P\left(z_i - \frac{\Delta z}{2}\right)}{P\left(z_i + \frac{\Delta z}{2}\right)} = e^{\left(\frac{Mg(z_i)}{RT(z_i)}\right)\Delta z} \tag{2.8}$$

The temperature is expressed by:

$$T(z_i) = \frac{Mg(z_i)\Delta z}{\left(\frac{RLogP(z_i - \frac{\Delta z}{2})}{P(z_i + \frac{\Delta z}{2})}\right)} \tag{2.9}$$

The density profile was measured up to the nth-layer of the atmosphere from approximately 72 km in campaign one, and approximately 60 km in campaign two. Hauchercorne et al. (1980) indicate that the pressure at the top (the higher layer of vertical observation) is fitted with the pressure of the MSIS-90 model. We fill the parameters of the relation

$P_m\left(z_n+\frac{\Delta z}{2}\right)$ with the desired month and latitude of observation using MSIS-90 model. The pressure in the top and bottom of the ith-layer is given by:

$$P\left(z_i+\frac{\Delta z}{2}\right)=\sum_{j=i+1}^{n}\rho(z_j)g(z_j)\Delta z+P_m\left(z_n+\frac{\Delta z}{2}\right), \tag{2.10}$$

$$P\left(z_i-\frac{\Delta z}{2}\right)=P\left(z_i+\frac{\Delta z}{2}\right)+\rho(z_i)g(z_j)\Delta z \tag{2.11}$$

respectively. Let X:

$$X=\frac{\rho(z_i)g(z_i)\Delta z}{P\left(z_i+\frac{\Delta z}{2}\right)} \tag{2.12}$$

The X parameter represents a ratio of experimental density values. The temperature is determined by:

$$T(z_i)=\frac{Mg(z_i)\Delta z}{RLog(1+X)} \tag{2.13}$$

The temperature has a statistical standard error of:

$$\frac{\delta T(z_i)}{T(z_i)}=\frac{\delta Log\left|1+X\right|}{Log\left|1+X\right|}=\frac{\delta X}{(1+X)Log(1+X)}\,. \tag{2.14}$$

Working equation (2.14) by:

$$\left(\frac{\delta X}{X}\right)^2 = \left|\frac{\delta\rho(z_i)}{\rho(z_i)}\right|^2 + \left|\frac{\delta P\left(z_i + \frac{\Delta z}{2}\right)}{P\left(z_i + \frac{\Delta z}{2}\right)}\right|^2 , \tag{2.15}$$

we obtain,

$$\delta P\left(z_i + \frac{\Delta z}{2}\right)^2 = \sum_{j=i+1}^{n} \left|g(z_i)\delta\rho(z_j)\Delta z\right|^2 + \left|\delta P_m\left(z_n + \frac{\Delta z}{2}\right)\right|^2 . \tag{2.16}$$

The standard error due to the temperature uncertainty presented at the top of the profile decreases with altitude. The absolute temperature can be deduced even though density measurements are only relative [Hauchercorne et al., 1980].

3 Collection and Data Analysis

A continuous time signal can be quite accurately represented by samples taken at discrete points in time under reasonable constraints using Nyquist criteria. The Nyquist frequency is half the sampling frequency of a discrete signal. If the Nyquist frequency is greater than the bandwidth (defines as the maximum component frequency of the sampled signal) aliasing can be avoided. Aliasing refers to an effect that causes different signals to become indistinguishable when sampled [Bores, 2012]. The Nyquist frequency is a property of a discrete time system, not of a signal. Time is commonly the domain of a signal, leading to a Nyquist frequency in Hertz. In general, a reconstruction of a signal is possible when the sampling frequency is greater than twice the maximum frequency of the signal being sampled. In order to understand the selection of sampling periods, it is necessary to discuss the buoyant force concept.

3.1 The Buoyant Force

We talk about gravity wave when a restoring force of gravity is acting on a fluid parcel, which has been displaced from its equilibrium position. The fluid buoyancy is acting, instead the gravity. In this section, we used [Nappo, 2002] to explain the theory of the oscillation dynamic that could be presented in the atmosphere.

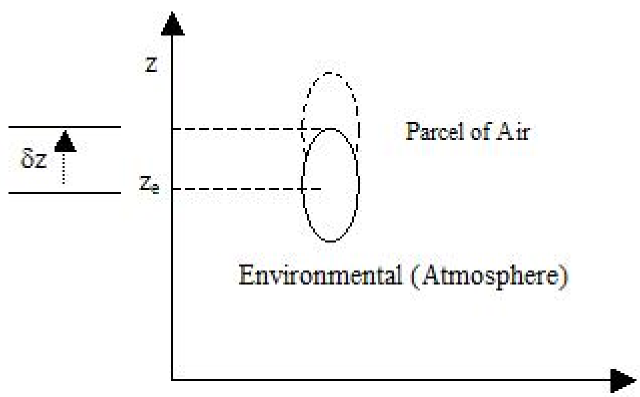

Figure 12: Behaviors for a Parcel of Air

Consider an environment (atmosphere at rest) and a parcel of air of mass m_p as shown in Figure 12. The air parcel is in equilibrium with its environment at height z_e. If the parcel is displaced upward a small distance δz from z_e, assuming the air in the parcel does not mix with the surrounding and experimenting an adiabatic process, there is not net transfer of heat across the surface of the air parcel. The buoyant force $\vec{F}_b$, acting on the fluid parcel is:

$$\vec{F}_b = -g\left(m_p - m_a\right)\hat{z}\,. \tag{3.1}$$

The mass of air displaced (environmental) by the fluid parcel is m_a, and the acceleration (positive upward) of gravity is g. Using the second law of motion,

$$m_p \frac{d^2(\delta z)}{dt^2} = -g\left(m_p - m_a\right). \tag{3.2}$$

We can express the mass of each air parcel as,

$$m_p = \rho_p \upsilon_p . \tag{3.3}$$

The density is ρ_p and the volume of the air parcel is υ_p. It is assumed that the volumes of the air parcel and the displaced air are equal and that the pressure in the air parcel is always equal to the environmental pressure. For dry air the ideal gas law, equation (3.4), represents the equation of state.

$$p = \rho RT . \tag{3.4}$$

The universal gas constant for dry air is R = 287J kg^{-1} K^{-1}. Combining (3.4) and (3.2) we obtain:

$$\frac{d^2(\delta z)}{dt^2} = -g\frac{\rho_p - \rho_a}{\rho_p} = -g\frac{T_a - T_p}{T_a} . \tag{3.5}$$

The environmental air density is ρ_a, T_a is the environmental temperature, and T_p is the parcel temperatures. Expanding T_a and T_p to first order:

$$T_a\left(z_e + \delta z\right) = T_0 + \left.\frac{\partial T_a}{\partial z}\right|_{z_e} \delta z + \ldots \tag{3.6}$$

$$T_p\left(z_e + \delta z\right) = T_0 + \left.\frac{\partial T_p}{\partial z}\right|_{z_e} \delta z + \ldots \tag{3.7}$$

The temperature at equilibrium height z_e is T_0. Inserting (3.6) and (3.7) in (3.5), we note that the change of environmental temperature due to the vertical displacement is small $T_0 >> \frac{\partial T_a}{\partial z}\delta z$.

The equation (3.5) becomes in:

$$\frac{d^2(\delta z)}{dt^2} = -\frac{g}{T_a}\left(\frac{\partial T_a}{\partial z} - \frac{\partial T_p}{\partial z}\right)\delta z\,. \tag{3.8}$$

If we set,

$$-\frac{\partial T_p}{\partial z} = \frac{g}{c_p} = \Gamma\,, \tag{3.9}$$

where c_p is the specific heat capacity at constant pressure and the adiabatic lapse rate is Γ. Equation (3.10) is the atmospheric temperature gradient.

$$\frac{\partial T_a}{\partial z} = \gamma_a \tag{3.10}$$

Then, equation (3.8) can be written as:

$$\frac{d^2(\delta z)}{dt^2} = -\frac{g}{T_a}(\Gamma - \gamma_a)\delta z\,. \tag{3.11}$$

The potential temperature is defined by:

$$\theta = T_a\left(\frac{1000}{p}\right)^{\frac{R}{c_p}}. \tag{3.12}$$

If a parcel of air were brought down adiabatically from height where the pressure is p to a height where the pressure is 1000 mb, the ground surface, the temperature would have it is the potential temperature [Nappo, 2002]. With the logarithmic derivative of equation (3.12) and using equation (3.4) with the hydrostatic approximation,

$$\frac{\partial p}{\partial z} = -\rho g \,, \tag{3.13}$$

we obtain,

$$\frac{1}{\theta}\frac{\partial \theta}{\partial z} = \frac{1}{T_a}\left(\frac{\partial T_a}{\partial z} - \frac{g}{c_p}\right) = \frac{\Gamma - \gamma_a}{T_a} \,. \tag{3.14}$$

Using equations (3.14) and (3.11), results in:

$$\frac{d^2(\delta z)}{dt^2} = -\frac{g}{\theta}\frac{\partial \theta}{\partial z}\delta z \,. \tag{3.15}$$

The equation of the simple harmonic motion in the vertical direction is represented by the equations (3.11) and (3.15). The motion of an air parcel if it is displaced vertically and released is described by:

$$\delta z(t) = Ae^{iNt} + Be^{-iNt} \,, \tag{3.16}$$

where a real N is the frequency of oscillation of the air parcel called the Brunt Vaisala frequency [Nappo, 2002], represented by:

$$N = \sqrt{\left(\frac{g}{\theta}\frac{\partial \theta}{\partial z}\right)} \,. \tag{3.18}$$

For gravity waves propagating at an angle to the vertical, we have:

$$N' = \left[\frac{g}{\theta} \frac{\partial \theta}{\partial z} \sin^2 \beta \right]^{\frac{1}{2}} = N \sin \beta \ . \tag{3.19}$$

The maximum frequency for vertically propagating gravity waves is represented by the Brunt Vaisala frequency [Nappo, 2002]. The Brunt Vaisala frequency $N \approx 0.02 s^{-1}$, and the buoyancy period is about 5 minutes in an isothermal atmosphere, where $\partial T / \partial z = 0$. Studies in 1986 confirmed a minimal buoyancy period in the atmosphere of about five minutes [Strauch et al., 1986].

Applying the sampling theory previously explained, results in a minimal frequency for the middle atmosphere of 0.2Hz. Therefore, the sampling frequency has to be at least 0.4 Hz. We need at least 2.5 minutes to reconstruct a signal with a period of five minutes. The Figure 13 shows an example of the Brunt Vaisala frequency, which presents the range about approximately five minutes of minimal wave periodicity for December 17, 2009 in the middle atmosphere, validating the results of Strauch et al., (1986).

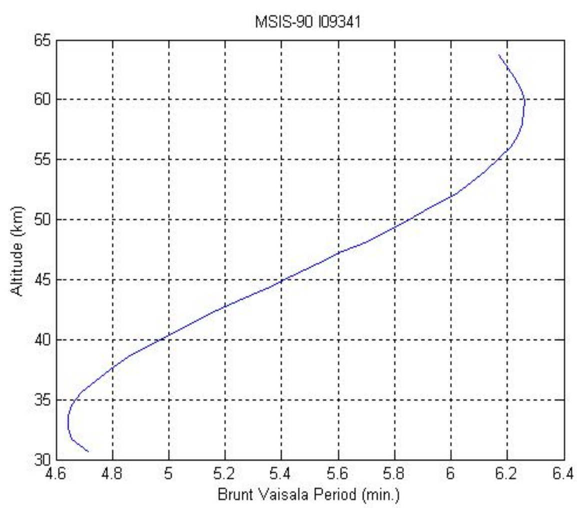

Figure 13: Brunt Vaisalla Frequency

3.2 Fourier Analysis

Often the frequency analysis of a signal is limited on resolution between different frequencies, limiting the opportunity to detect a small signal in the presence of a large one. The limitation in resolution arises because the signal can only be measured for a limited period of time. Fourier series assume that the analyzed signal is repetitive. Because most signals will have discontinuities at the measured initial and end time, the Fourier transform will assume discontinuities that are not really there. If sharp discontinuities have broad frequency spectra, this will cause the frequency spectrum of the signal to be spread out [Bores, 2012]. The spreading is the result that the energy should be concentrated only at one frequency instead leaks into all the other frequencies. This phenomenon of energy spreading is called ‘spectral leakage’. This problem is not related to the fact of having sampled the signal rather it is due to the finite nature of the measured time. The result is that any given spectral component will contain not just the signal energy, but also noise from the whole of the remainder of the spectrum. Furthermore the spectral leakage from a large signal component may be severe enough to mask other smaller signals at different frequencies.

The effect of measuring a finite time signal is equivalent to multiplying the signal by a rectangular function of unit amplitude. The finite measurement time is called a ‘window’. The idea leads to the rectangular function being called a ‘rectangular window’. The effect of spectral leakage is reduced by reducing the discontinuities at the end of the measured signal, multiplying for a window that smoothes the signal to zero at the ends.

The digital prolate spheroidal sequence or Slepian window can be used to maximize the concentration of energy [Percival, 1993]. Percival explained the sequence importance in the windowing process as follows: “The sequence maximizing the ratio is the first discrete prolate spheroidal or Slepian sequence. The second Slepian sequence maximizes the ratio and is orthogonal to the first Slepian sequence. The third Slepian sequence maximizes the ratio of integrals and is orthogonal to both the first and second Slepian sequences. Continuing in this way, the Slepian sequences form an orthogonal set of band limited sequences.” Figure 14 shows a Slepian window, which provides the frequency domain concentration ratios nearly to one in the pass band. This was the window used in the spectral analysis of this project.

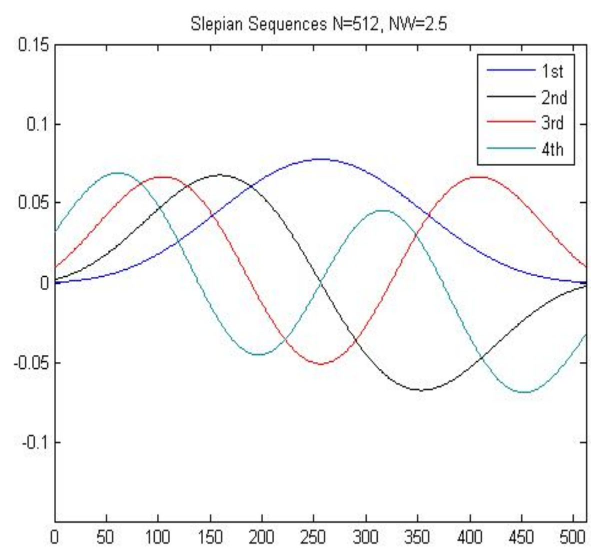

Figure 14: Discrete Prolate Spheroidal (Slepian) Sequences

The following procedure was used to implement the frequency analysis algorithm:

1. A smoothing function is applied to the data to discard outliers. A Savitzky-Golay (polynomial) smoothing filter was used to smooth the signal.
2. The mean temperature was subtracted from the observed temperatures.
3. Each time series fluctuation for the four windows of the DPSS was multiplied to remove the long-term trend from the time series fluctuations of the temperature data for a given altitude level.
4. The fast Fourier transform (FFT) was applied and the power spectral density (PSD) was obtained.
5. The fourth PDS result is averaged.
6. Fisher's test and Siegel's test are applied.

3.3 Standard Model Data

We used an atmospheric model available from the Goddard Space Flight Center, Nasa Space Physic Data Facility, called the MSIS-90 Model. See APPENDIX B – C. The model presents the neutral temperature and densities of the Earth's atmosphere from ground to thermosphere. We used the data obtained with this online model to trace the standard temperature vertical profile of the middle atmosphere in our region of interest. The MSIS-90 theoretical profiles offer a good standard to compare with the experimental Lidar data.

3.4 Raw Data Description

The first stage of our project consisted in observing time series of raw data for temperature profiles. We attempt to characterize the data, observe the sampling periods and the behavior of the data in time. We applied a probability plot to observe a normal distribution over the data. Figure 15 show an example of the normal distribution probability plot.

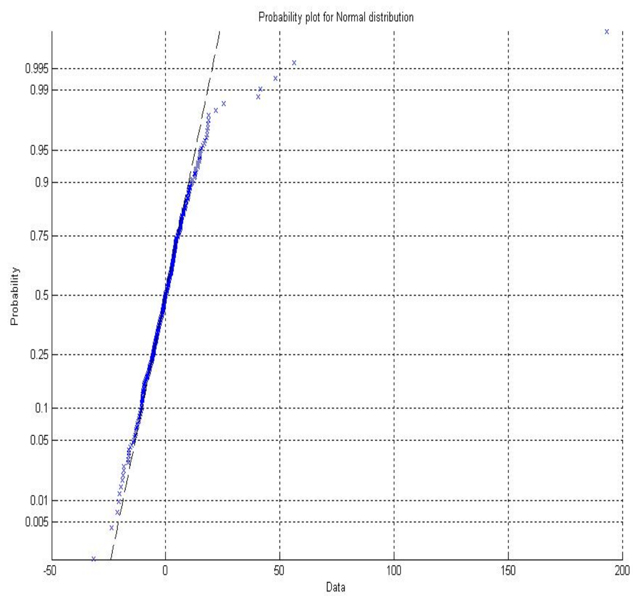

Figure 15: Probability plot for normal distribution

With the basic statistical analysis, we apply a spectral characterization, for the regular sampled data, and the unevenly sampled data. In the unevenly spaced cases, we also apply the Fisher test and Siegel test to detect periodicity. Figures 16 - 27 present examples of the raw data temperature fluctuations for the two campaigns. In the figures we can observe the data gaps, demonstrating the uneven sampling.

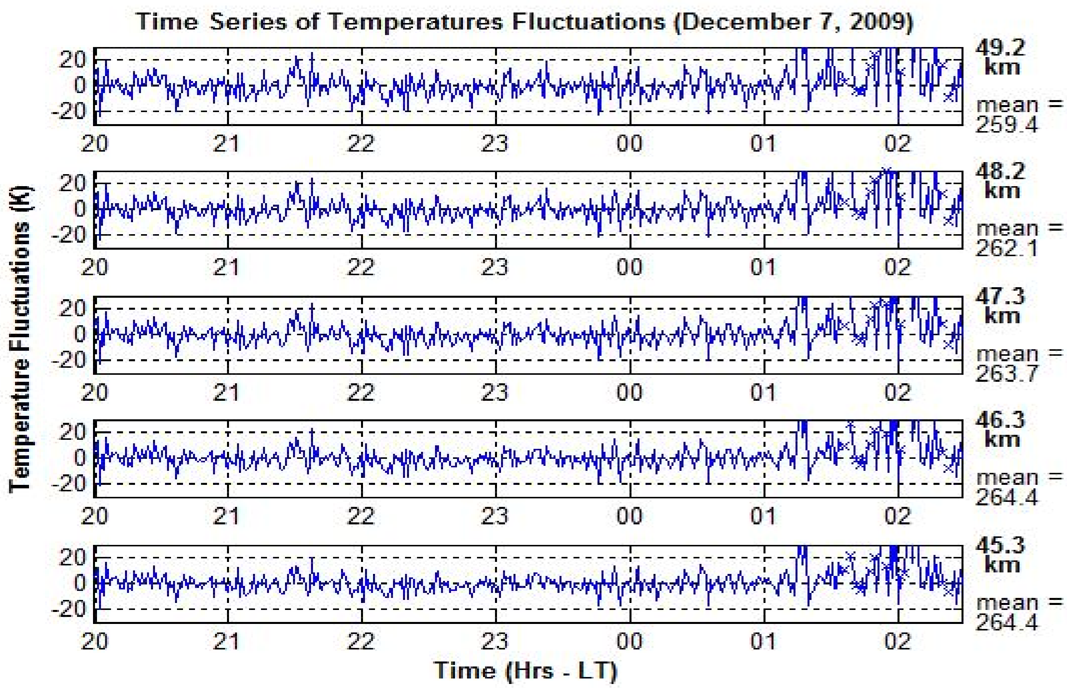

Figure 16: Time Series Fluctuations for December 7, 2009 (45.3 – 49.2 km)

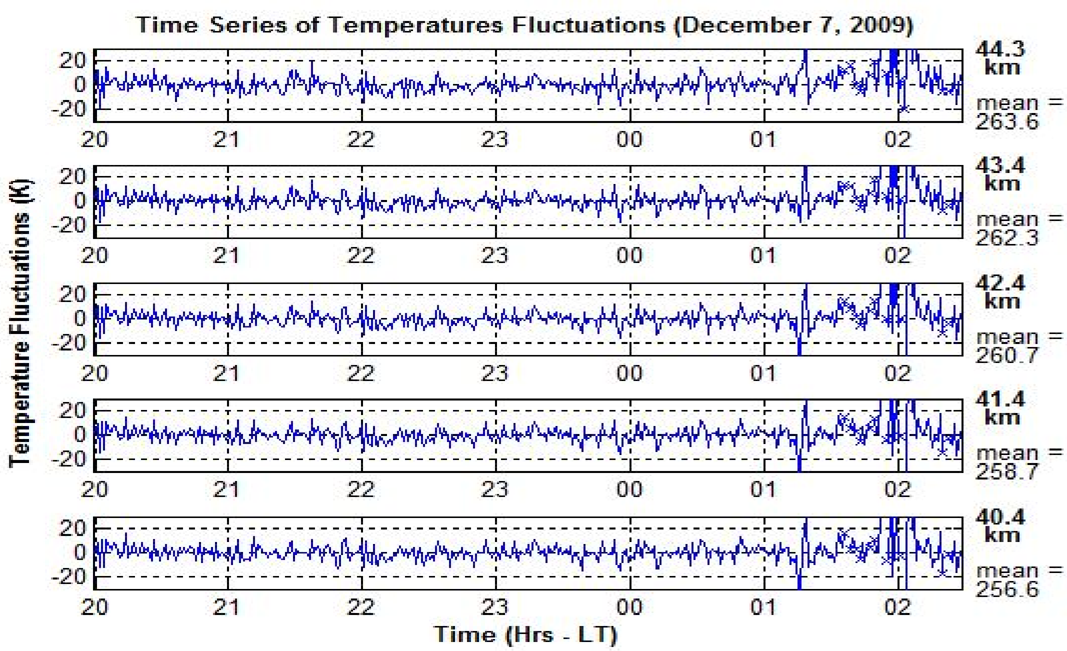

Figure 17: Time Series Fluctuations for December 7, 2009 (40.4 – 44.3 km)

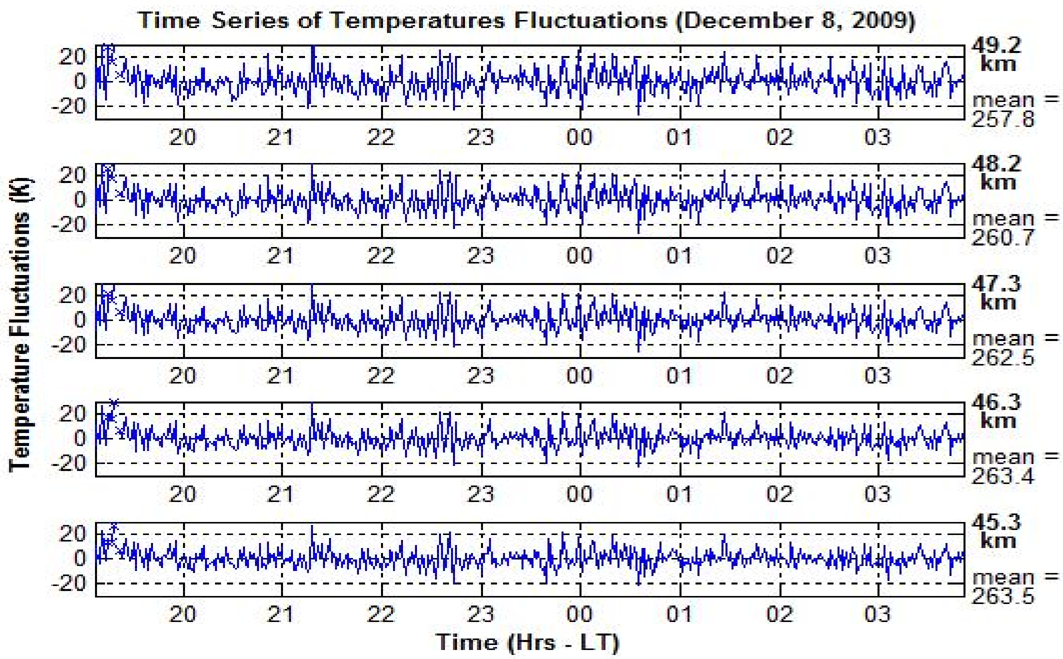

Figure 18: Time Series Fluctuations for December 8, 2009 (45.3 – 49.2 km)

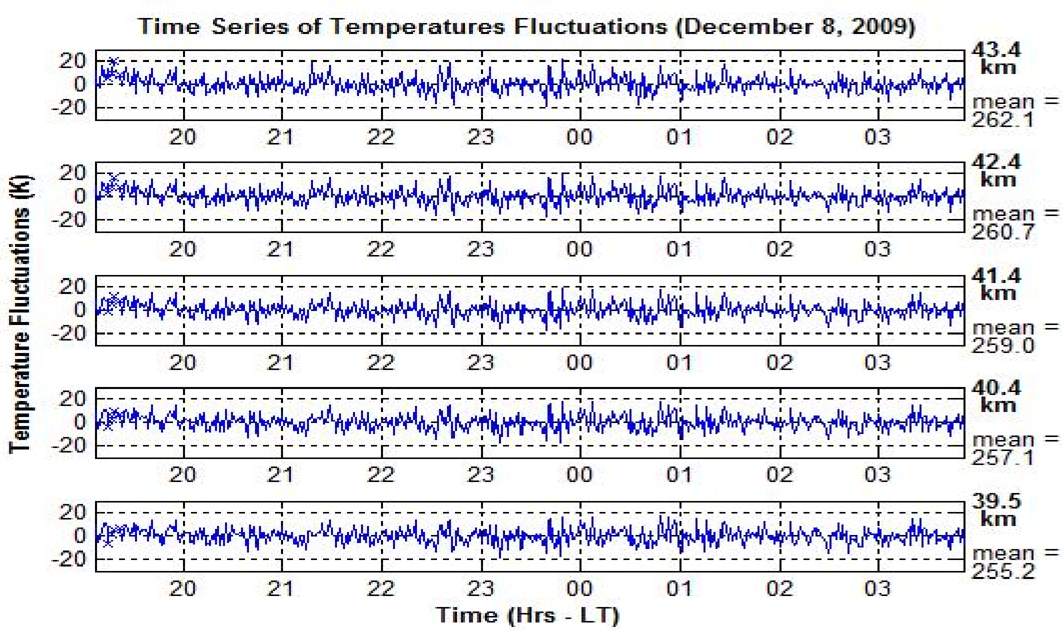

Figure 19: Time Series Fluctuations for December 8, 2009 (39.5 – 43.4 km)

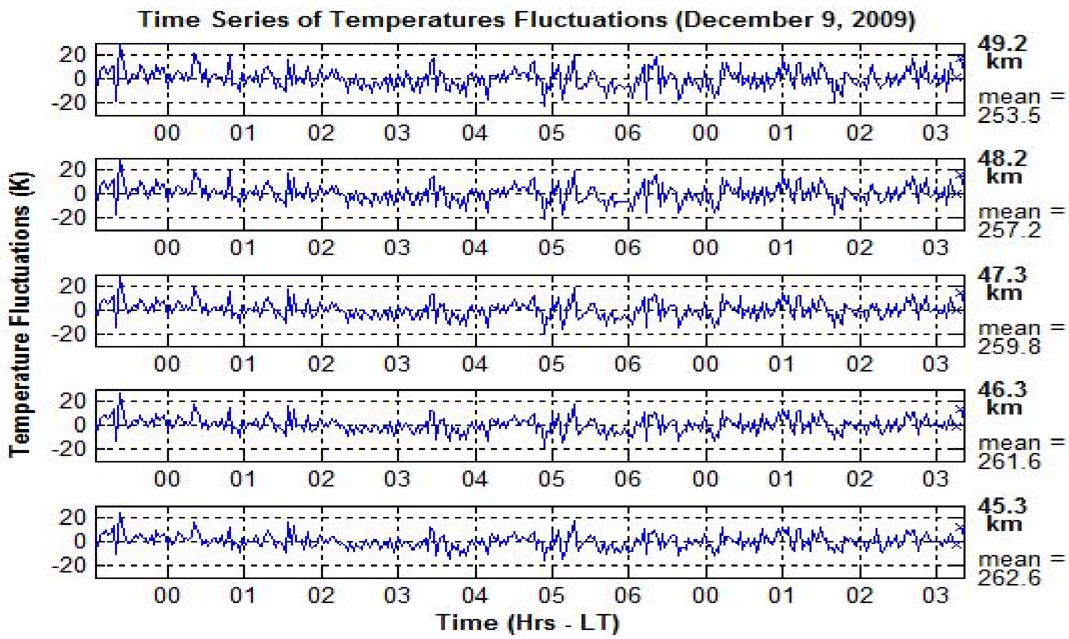

Figure 20: Time Series Fluctuations for December 9, 2009 (45.3 – 49.2 km)

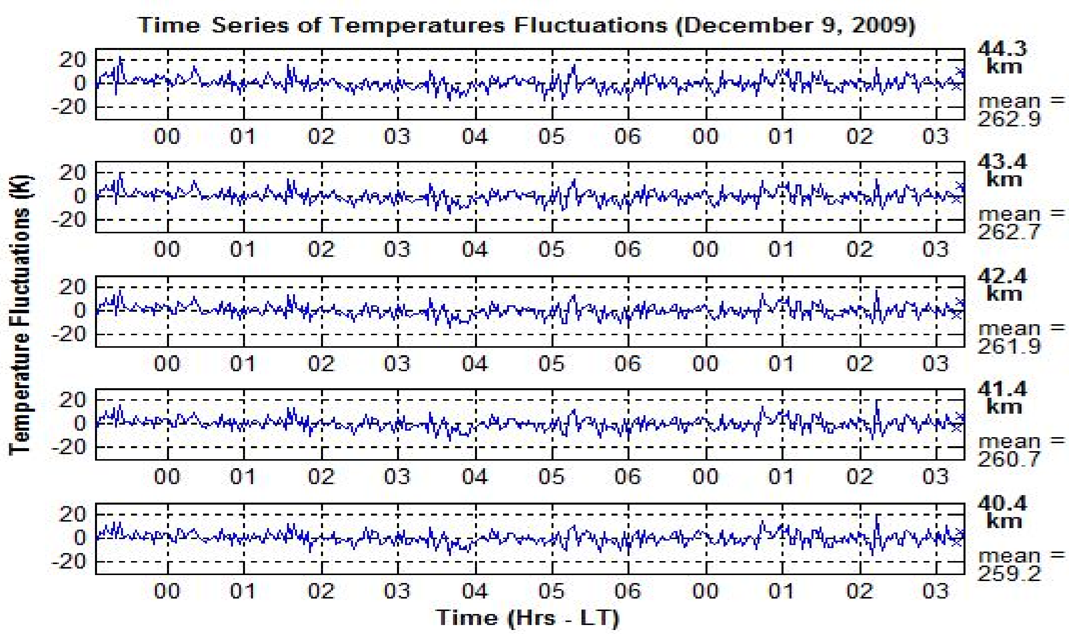

Figure 21: Time Series Fluctuations for December 9, 2009 (40.4 – 44.3 km)

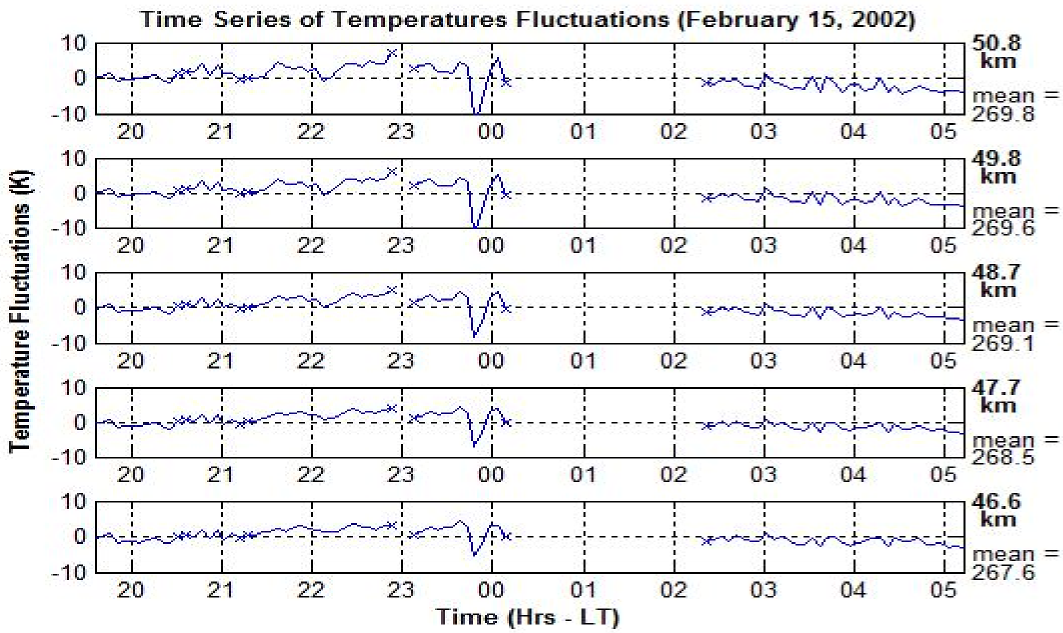

Figure 22: Time Series Fluctuations for February 15, 2002 (46.6 – 50.8 km)

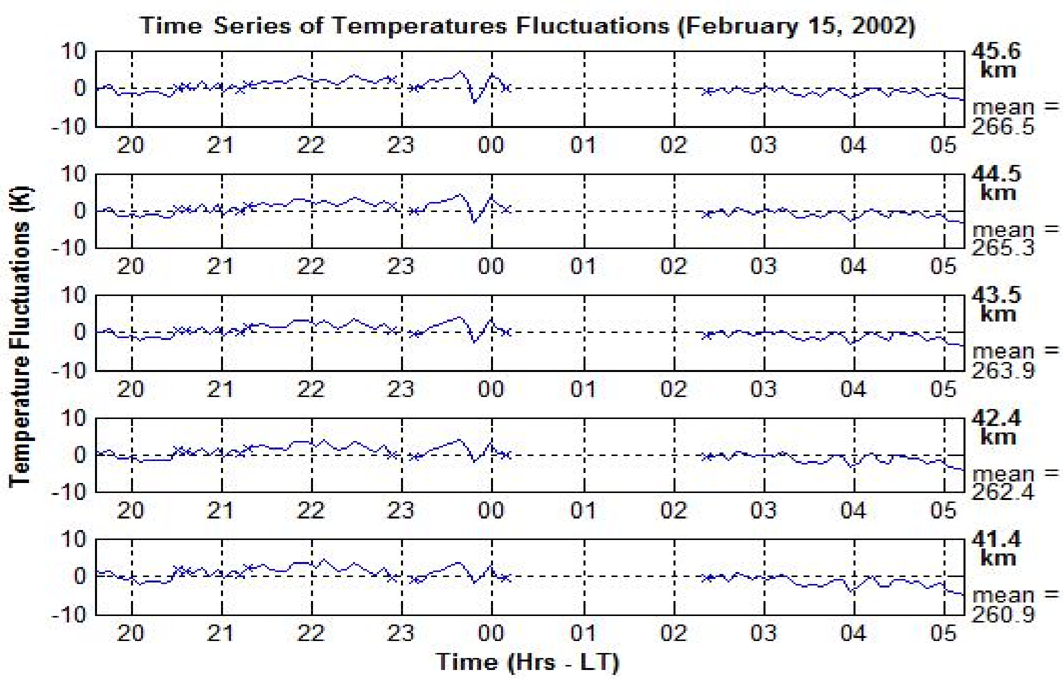

Figure 23: Time Series Fluctuations for February 15, 2002 (41.4 – 45.6 km)

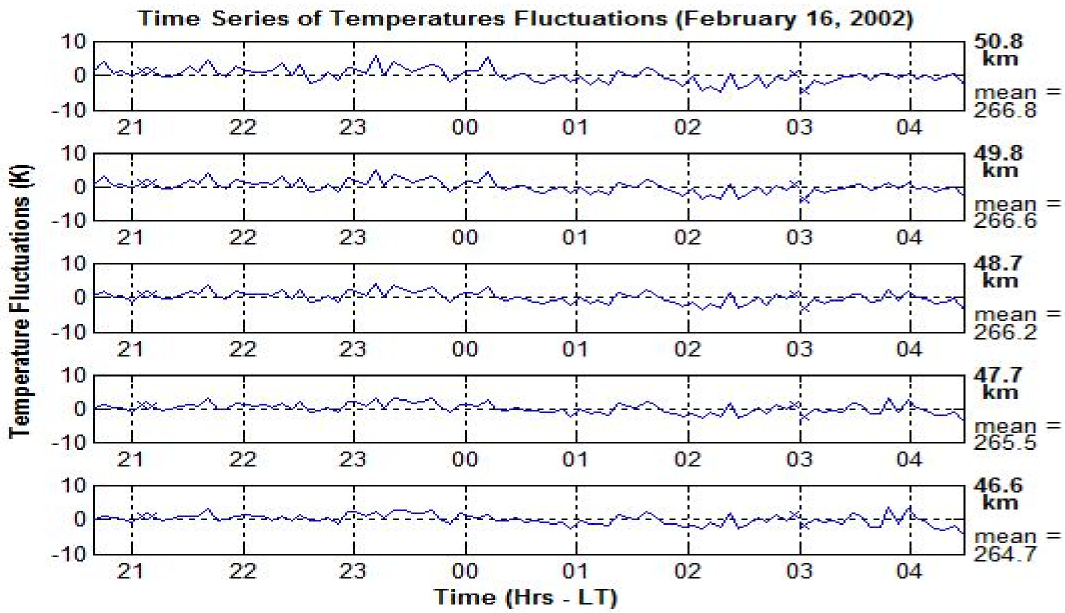

Figure 24: Time Series Fluctuations for February 16, 2002 (46.6 – 50.8 km)

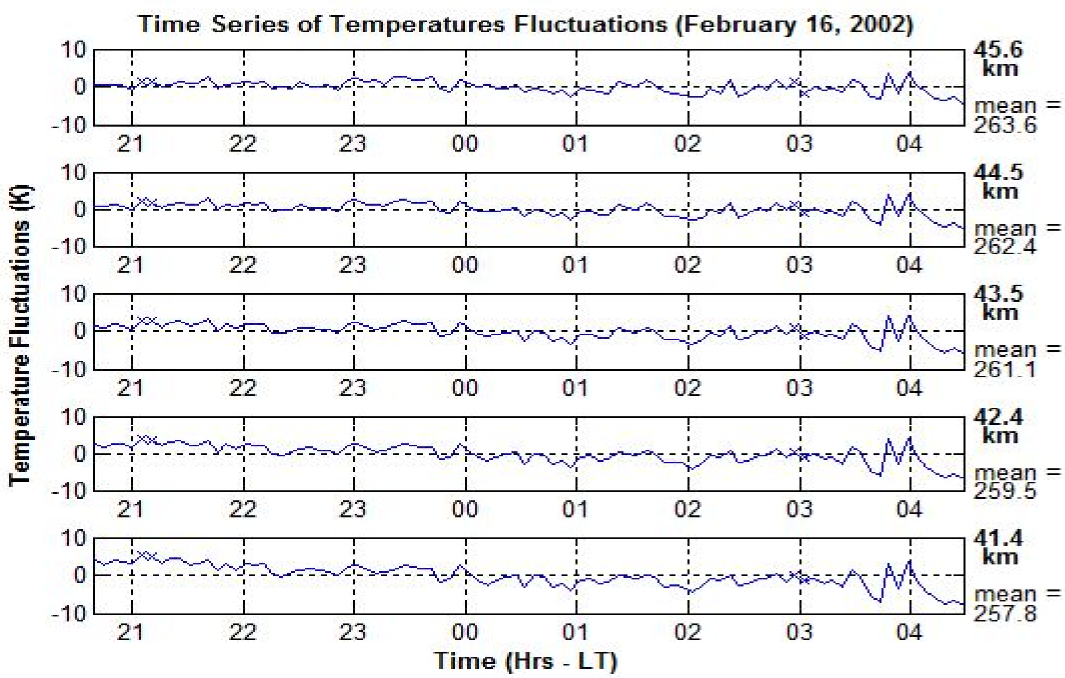

Figure 25: Time Series Fluctuations for February 16, 2002 (41.4 – 45.6 km)

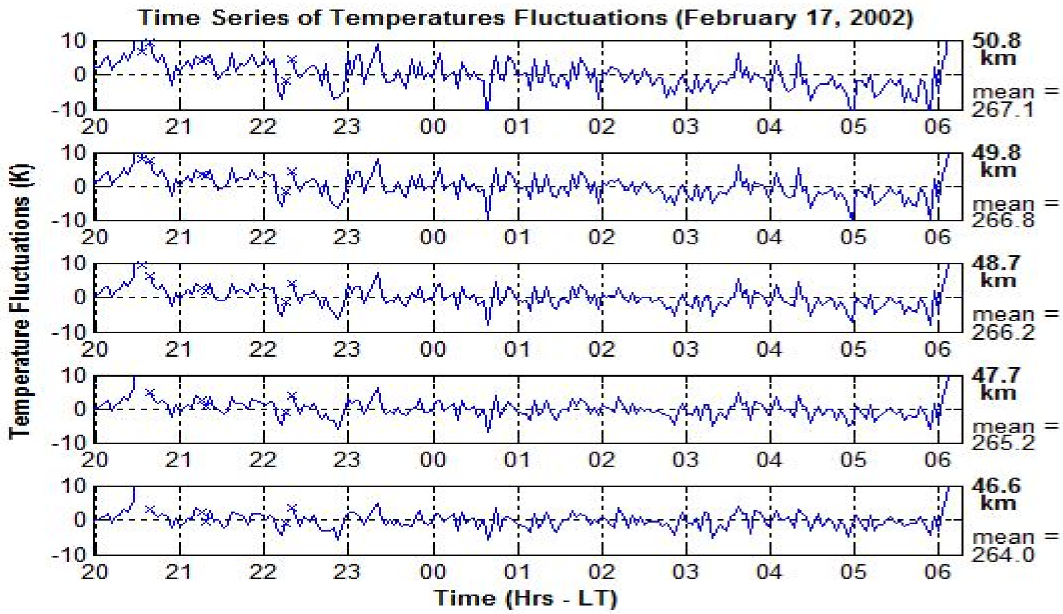

Figure 26: Time Series Fluctuations for February 17, 2002 (46.6 – 50.8 km)

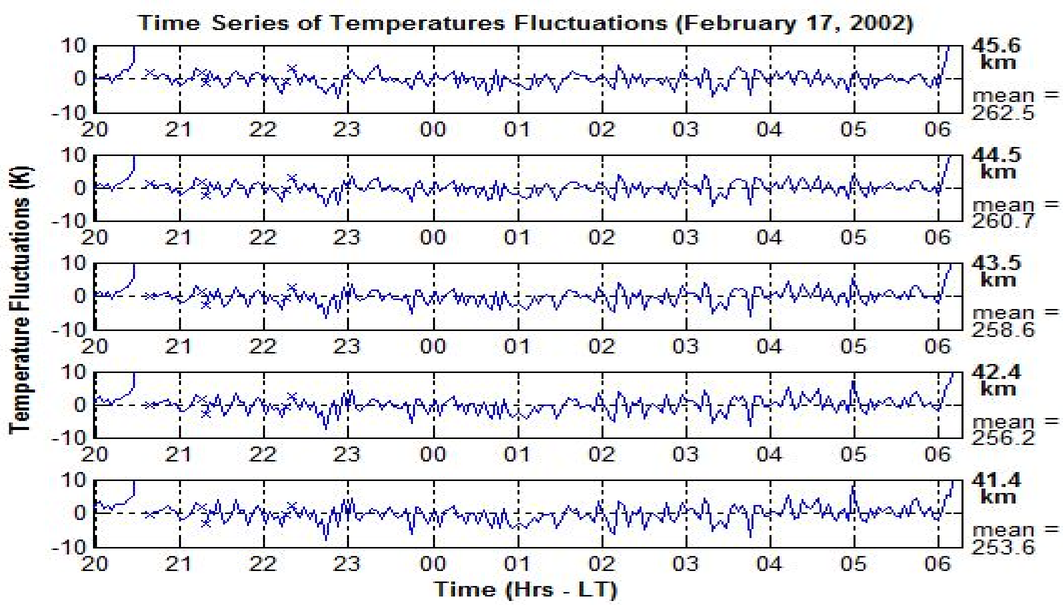

Figure 27: Time Series Fluctuations for February 17, 2002 (41.4 – 45.6 km)

3.5 Data Statistical Parameters

The data used for this project were obtained from two sources. We have experimental temperature profiles from a Lidar. We also have standard theoretical vertical temperature profiles obtained from MSIS-90 online application. A brief description of both is presented in the following sections.

3.5.1 Vertical Profile

A standard theoretical vertical temperature profile is obtained with the online MSIS-90 model presented above in section 3.3. This standard vertical profile is plotted with the vertical mean temperature profiles for the two data sets along with a fifth order polynomial fitting. Figure 26 and Figure 30 present the behavior of the three graphs, for the two campaigns. We can observe that from 30 to 35 km, Lidar observations indicate a heating compared with the vertical profile of the standard model for 2009 Campaign. Above 50 km the Lidar temperature profile reports a behavior very distant to the model for the 2009 data. Also, this error pattern is observed in Figures 4 – 6, above 50 km and several outliers are evident. In Figures 31 – 33 the temperature data descend to zero, a prominent bias in relation to the standard model. In Figure 28 we observe prominent outliers over 60 km. Standard deviations from the mean temperature profile are shown using error bars in Figures 34 – 39.

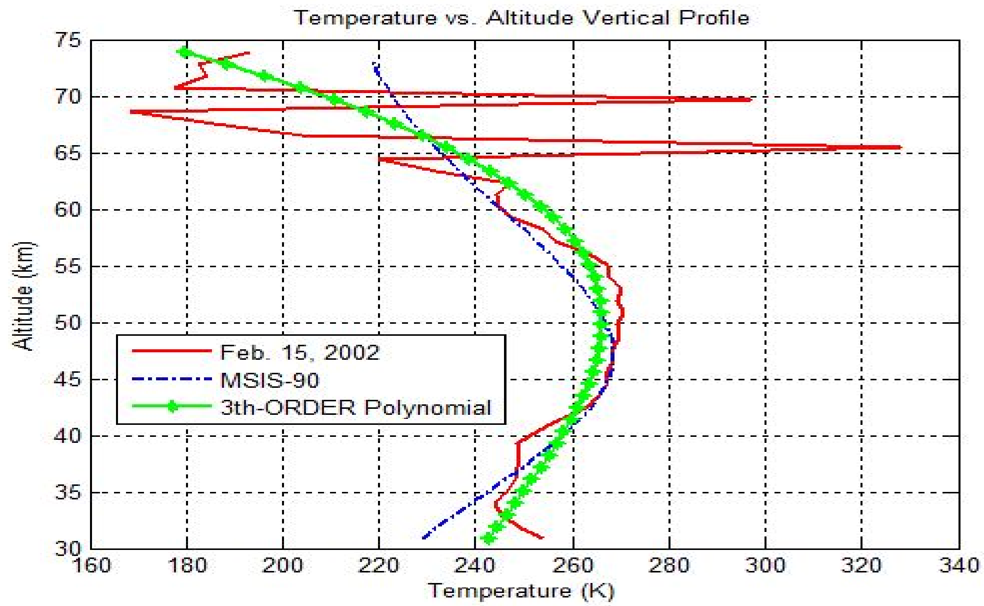

Figure 28: Vertical Profiles for February 15, 2002

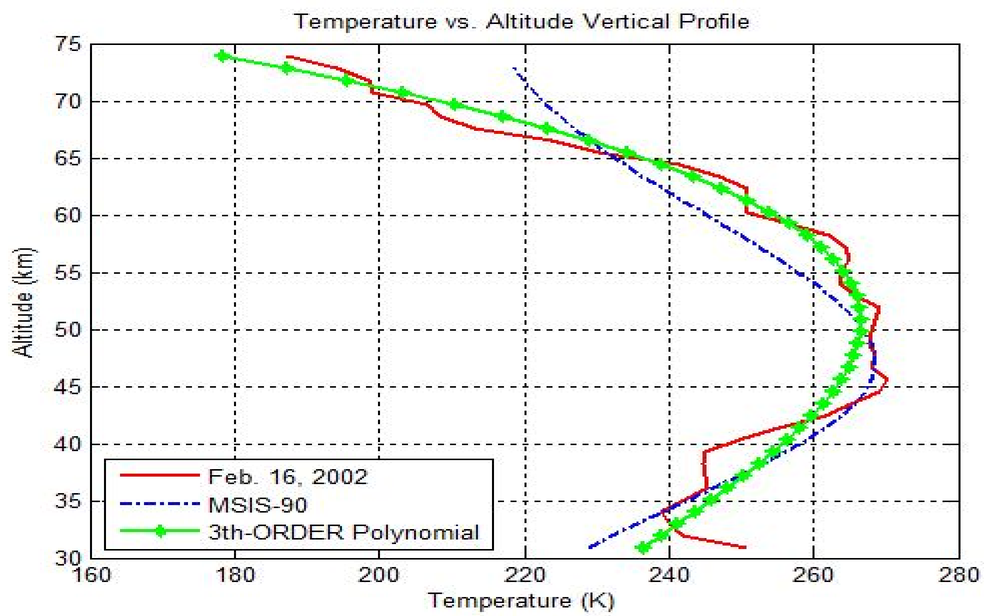

Figure 29: Vertical Profiles for February 16, 2002

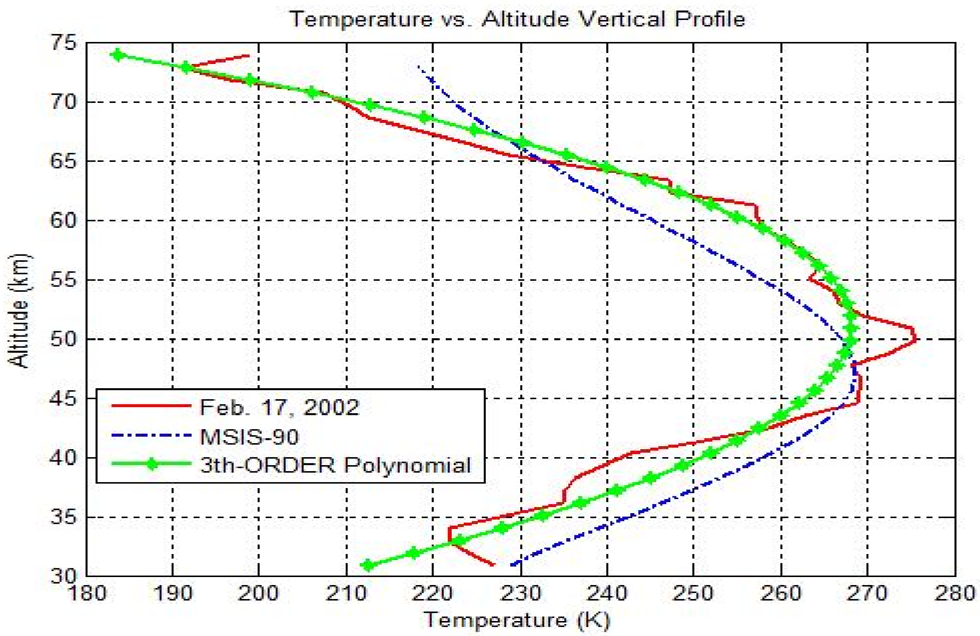

Figure 30: Vertical Profiles for February 17, 2002

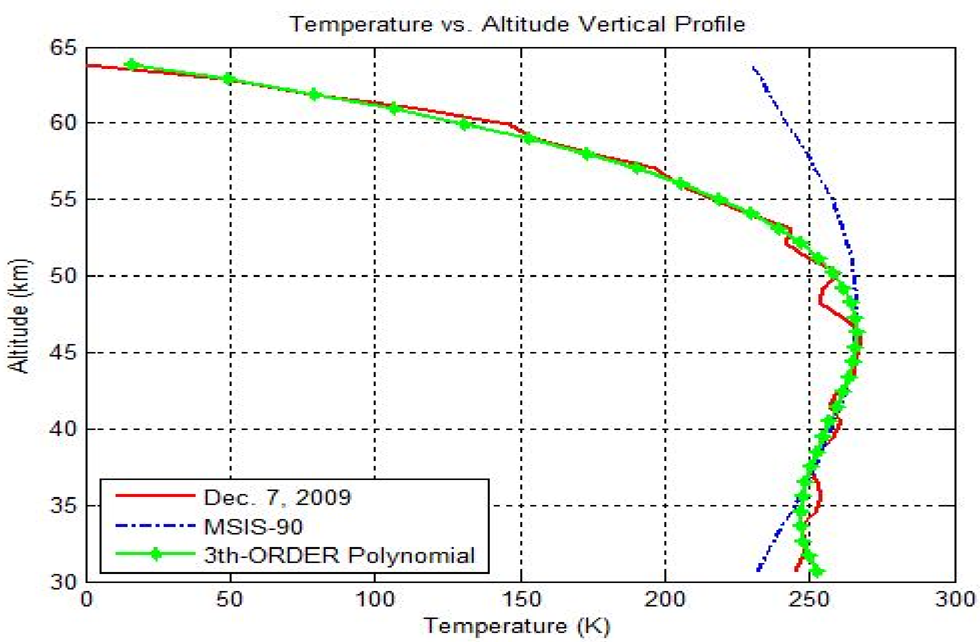

Figure 31: Vertical Profiles for December 7, 2009

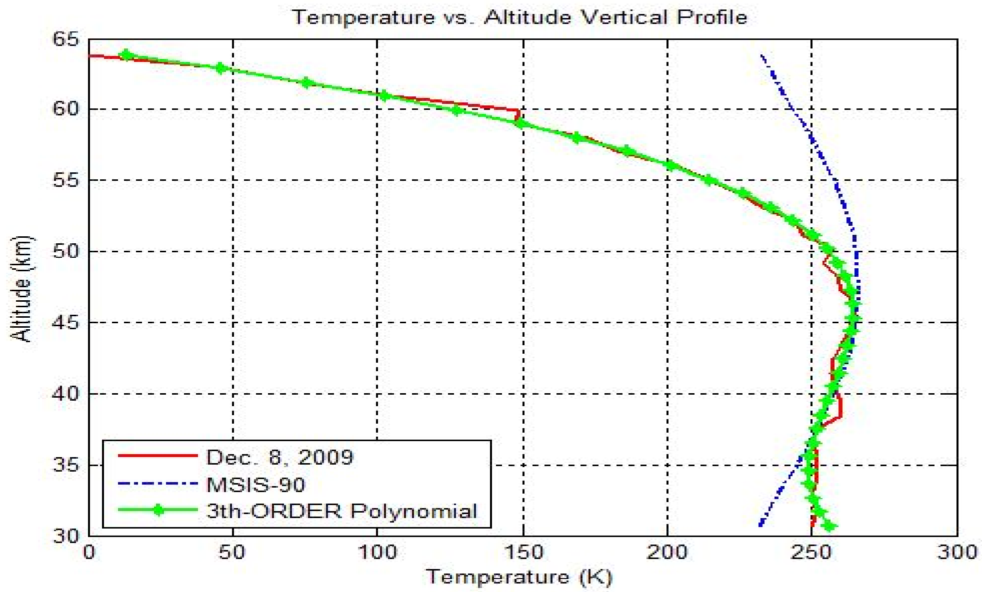

Figure 32: Vertical Profiles for December 8, 2009

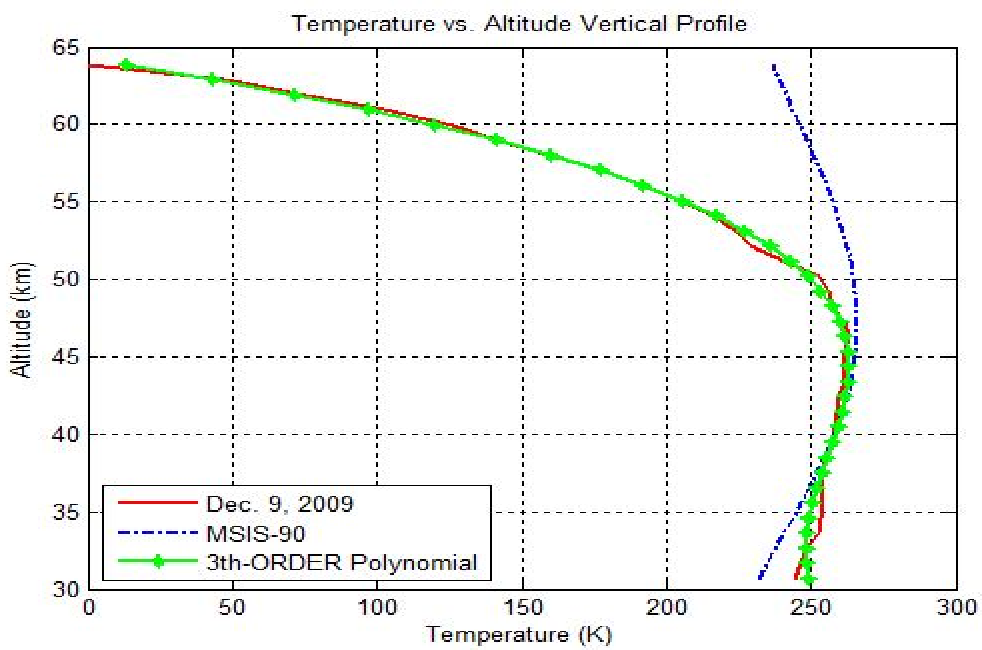

Figure 33: Vertical Profiles for December 9, 2009

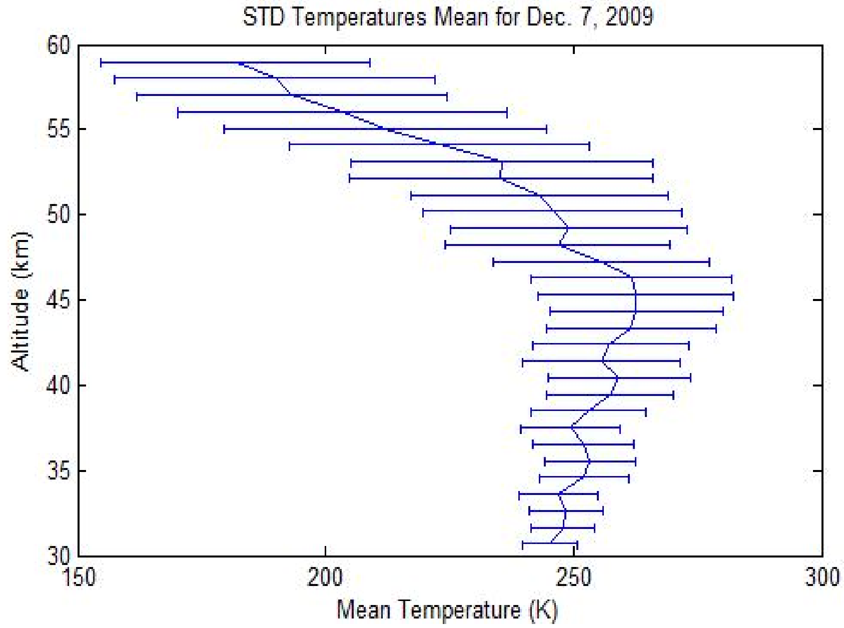

Figure 34: Standard Deviation for Mean Temperature – Dec. 7, 2009

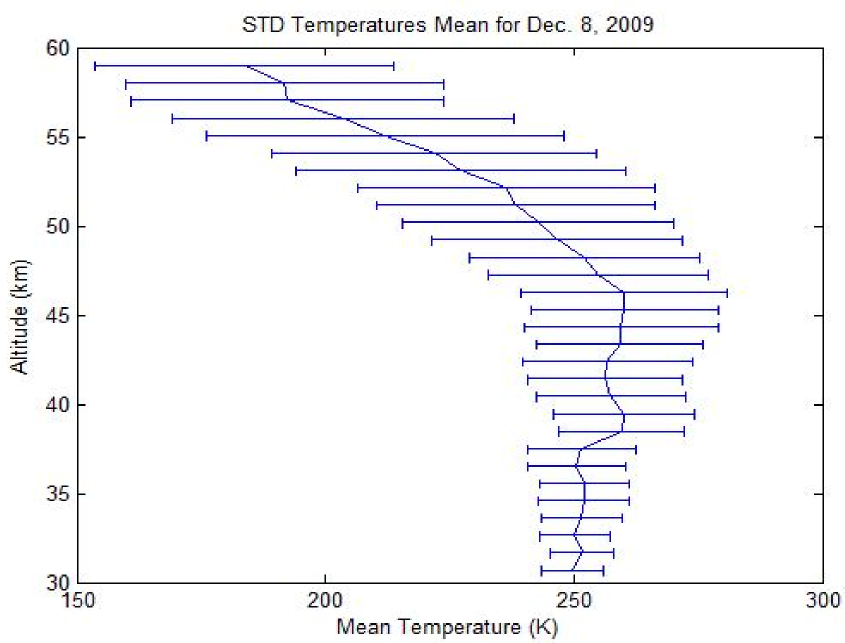

Figure 35: Standard Deviation for Mean Temperature – Dec. 8, 2009

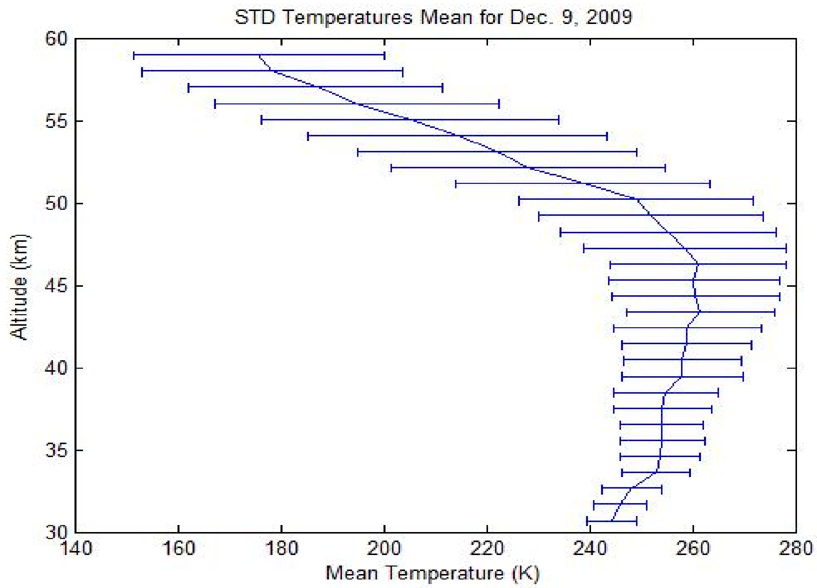

Figure 36: Standard Deviation for Mean Temperature – Dec. 9, 2009

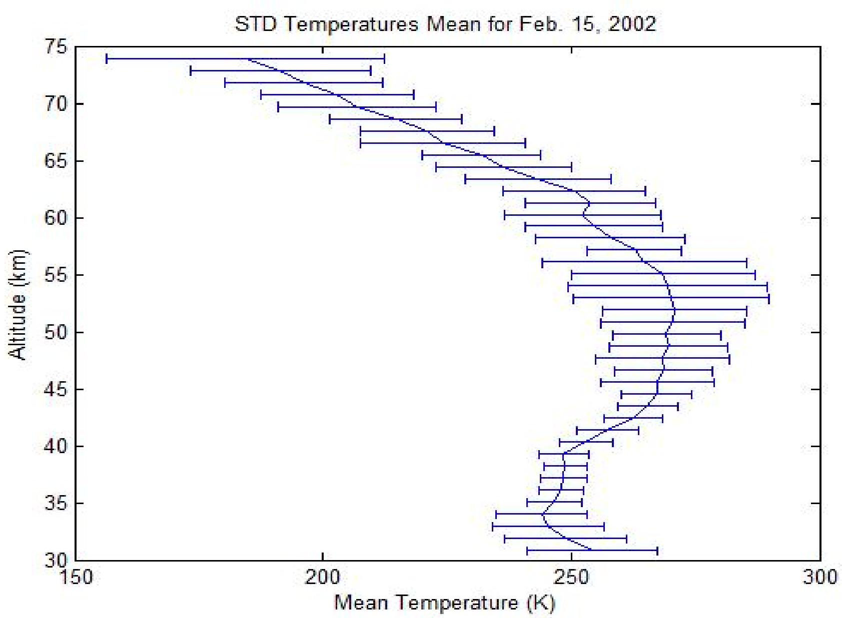

Figure 37: Standard Deviation for Mean Temperature – Feb. 15, 2002

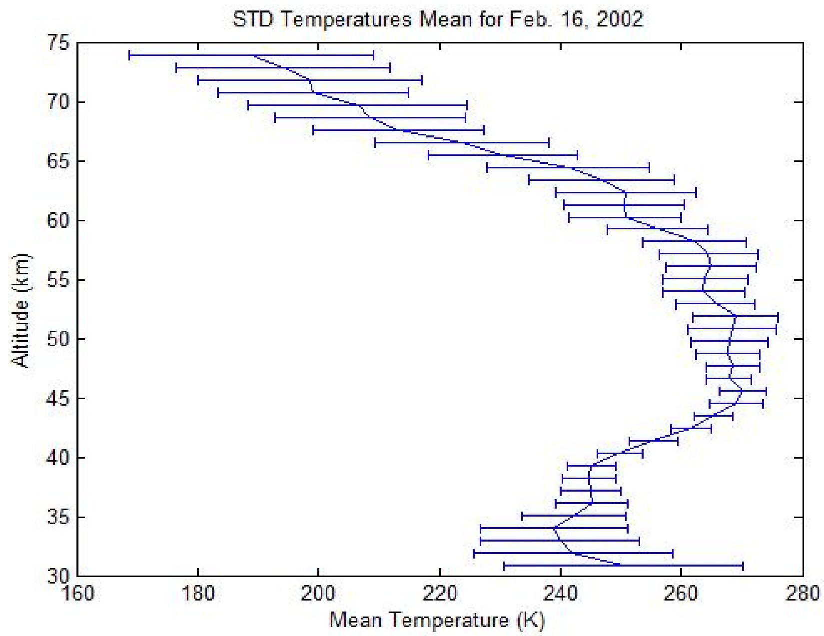

Figure 38: Standard Deviation for Mean Temperature – Feb. 16, 2002

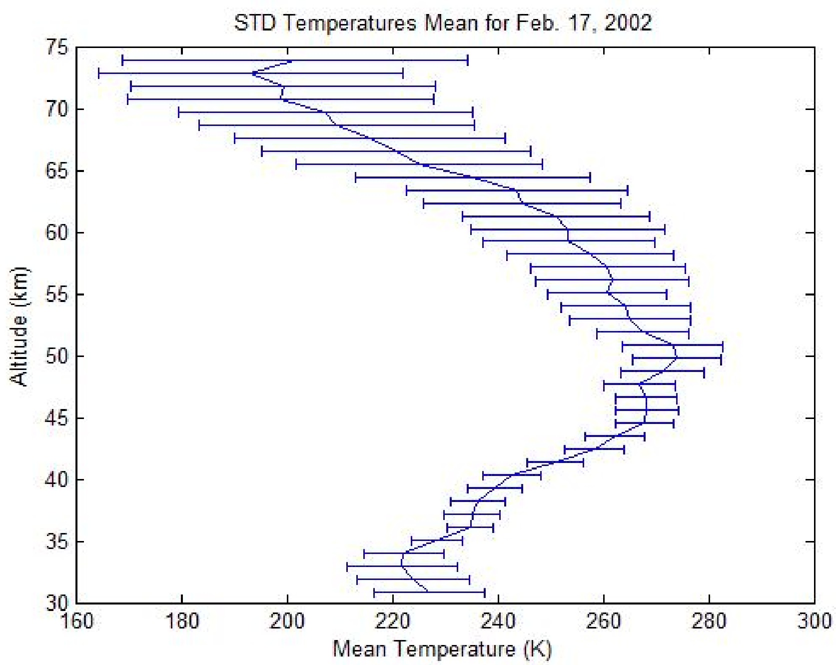

Figure 39: Standard Deviation for Mean Temperature – Feb. 17, 2002

Temperature time sequences with a 5° K offset are shown in Figures 40 - 45. We observe a downward phase progression in the range of 40 – 45 km for February 15 – 17. For the December campaign the downward phase progression is not visible.

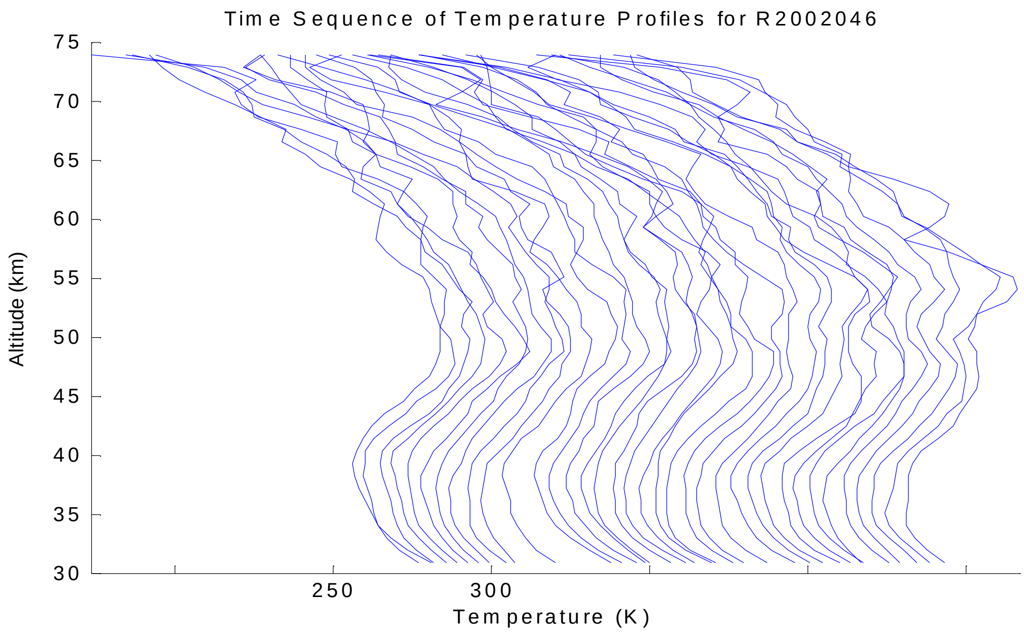

Figure 40: Time Sequence for February 15, 2002

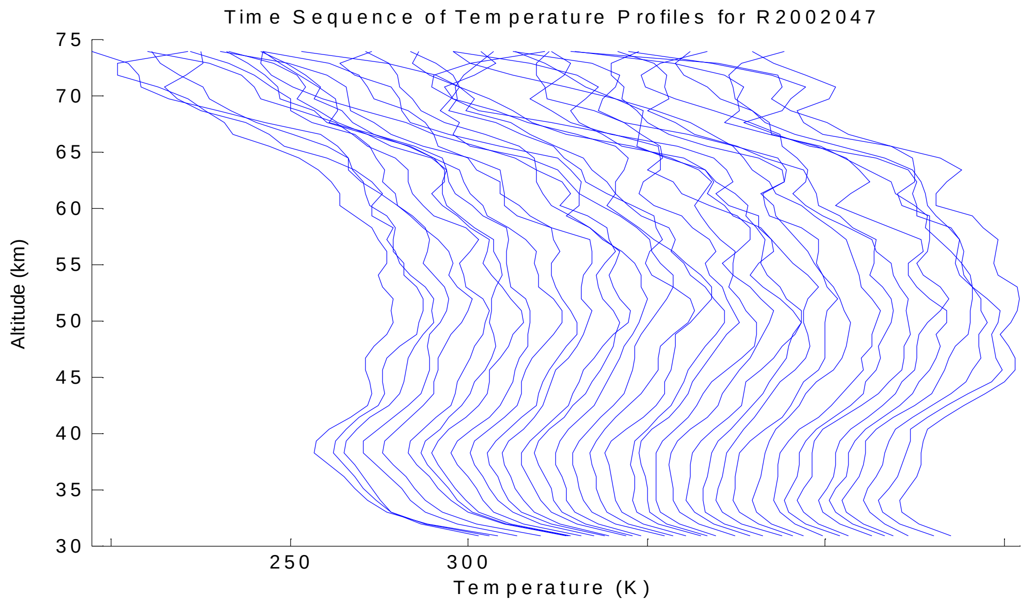

Figure 41: Time Sequence for February 16, 2002

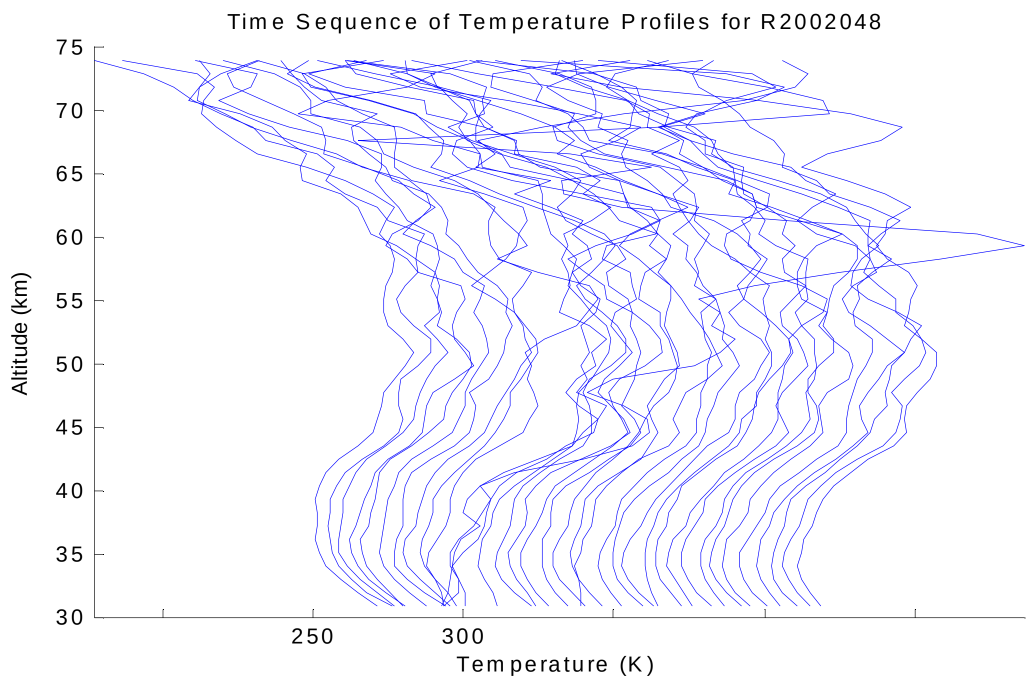

Figure 42: Time Sequence for February 17, 2002

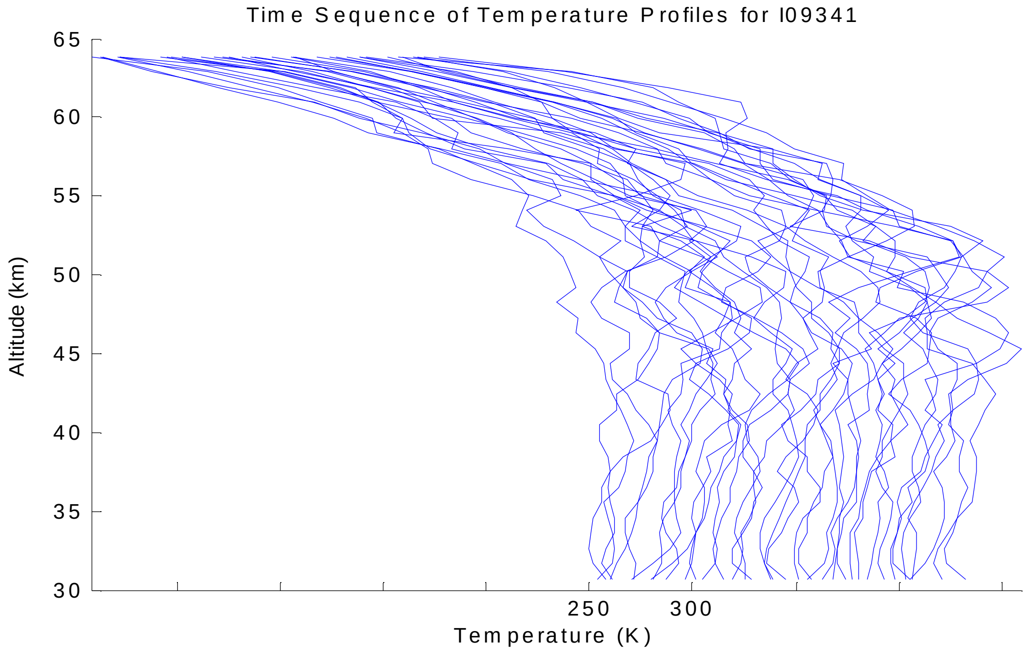

Figure 43: Time Sequence for December 7, 2009

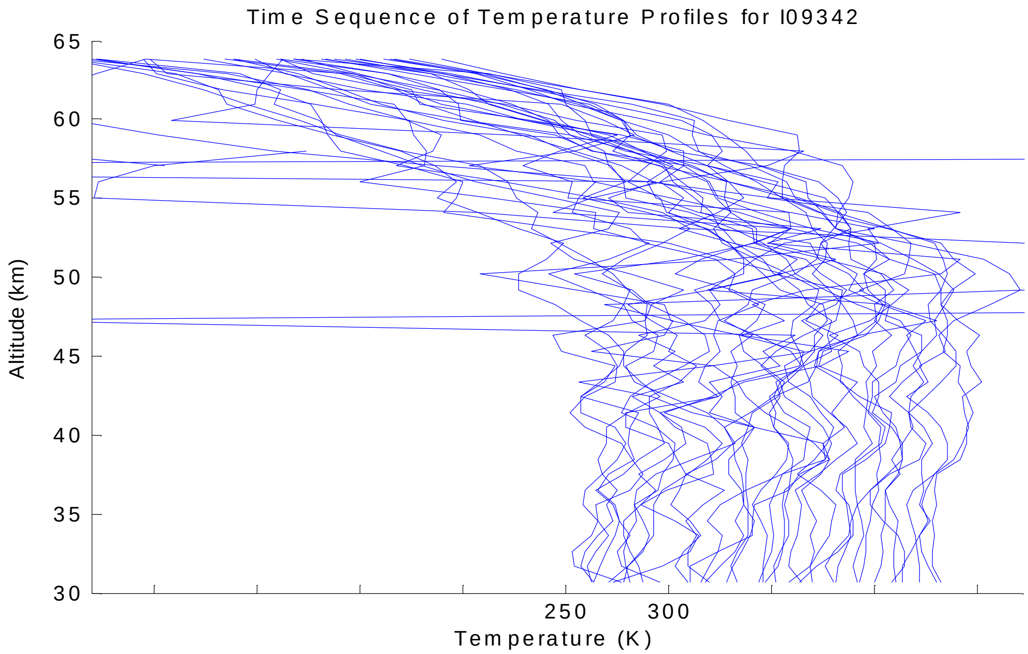

Figure 44: Time Sequence for December 8, 2009

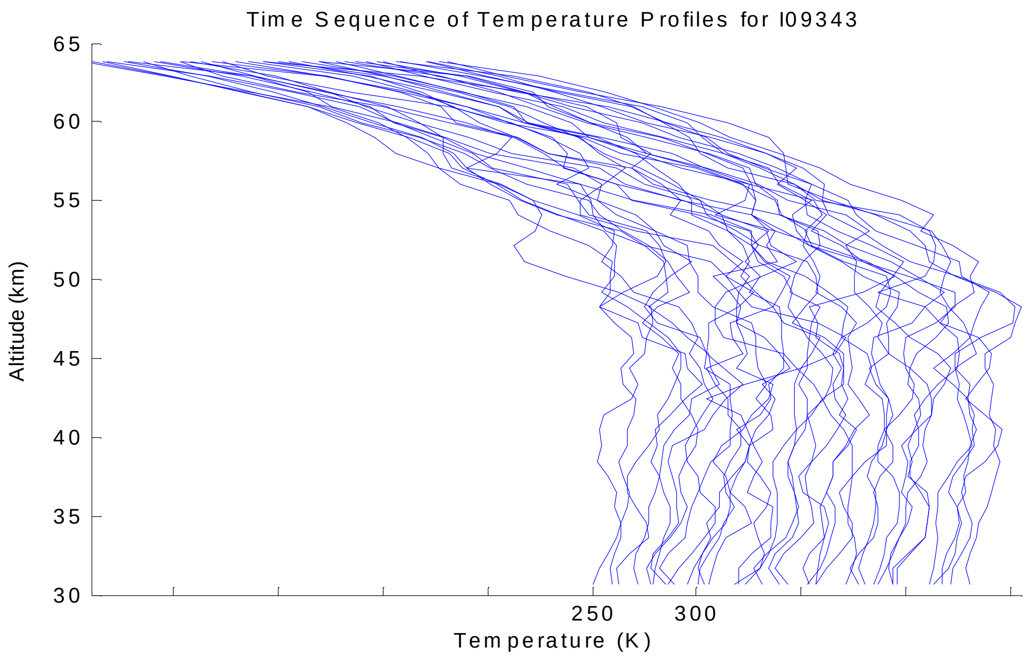

Figure 45: Time Sequence for December 9, 2009

3.5.2 Vertical Fluctuations

We decided to apply a third order polynomial to the vertical profile obtained from the Lidar observations. Then, the polynomial was subtracted from the vertical profile, leaving the fluctuations. Figures 46 - 53 are plots of the fluctuations. These figures were used to find the vertical wavelength. In Figures 50 – 52, for December 7 – 8, 2009, we observe a vertical wavelength of approximately 4 km in the range of 30 – 45 km. We consider that this vertical wave is the result of a low speed wave, known as an internal gravity wave.

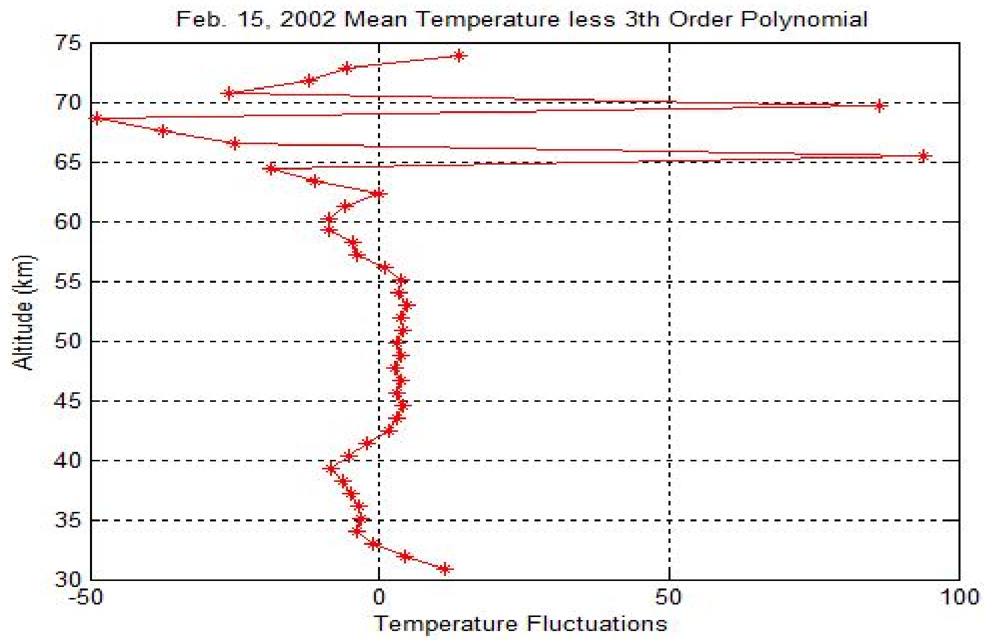

Figure 46: Vertical Fluctuations for February 15, 2002

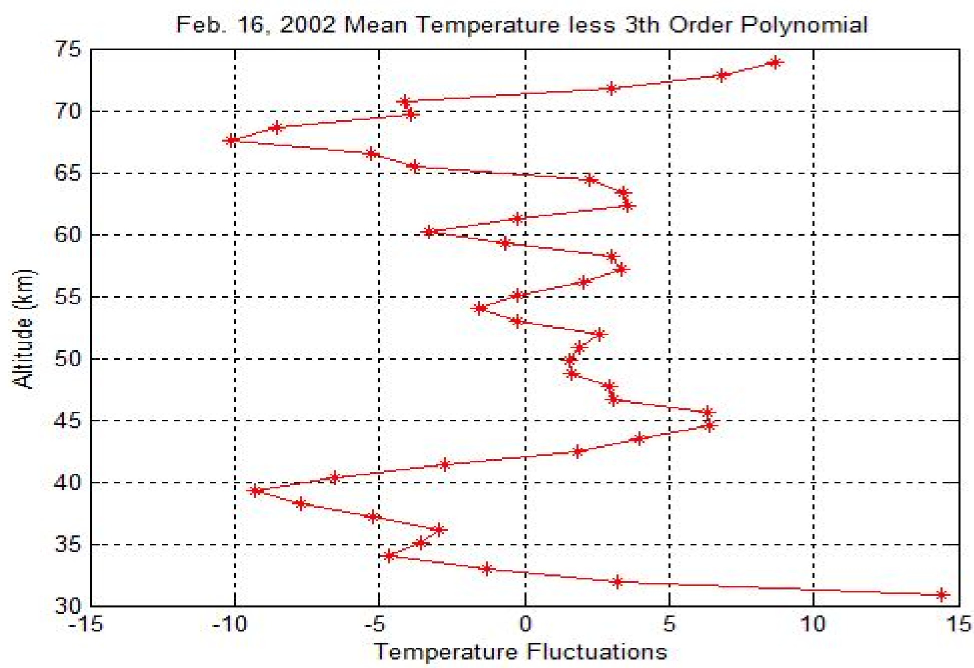

Figure 47: Vertical Fluctuations for February 16, 2002

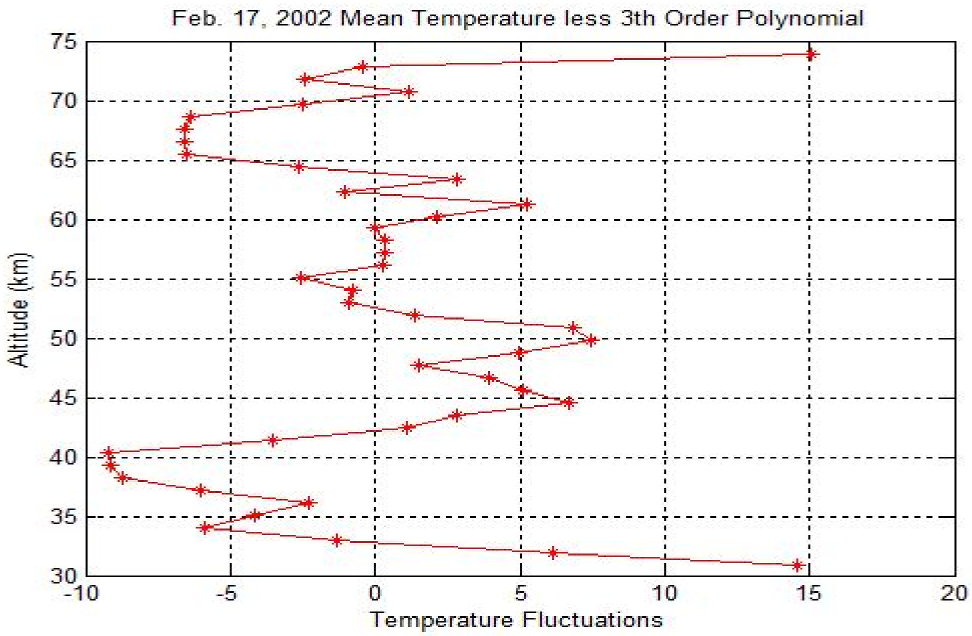

Figure 48: Vertical Fluctuations for February 17, 2002

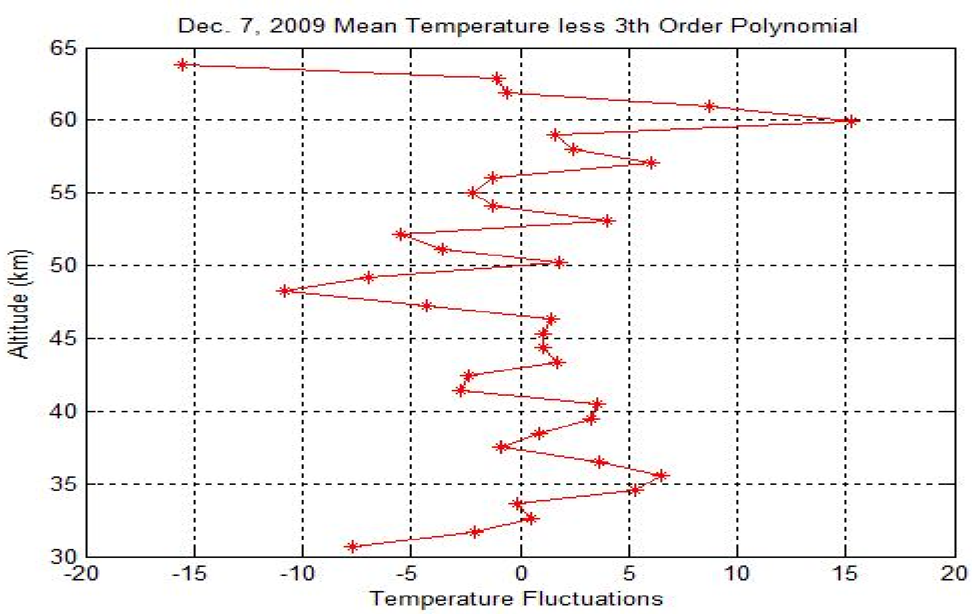

Figure 49: Vertical Fluctuations for December 7, 2009

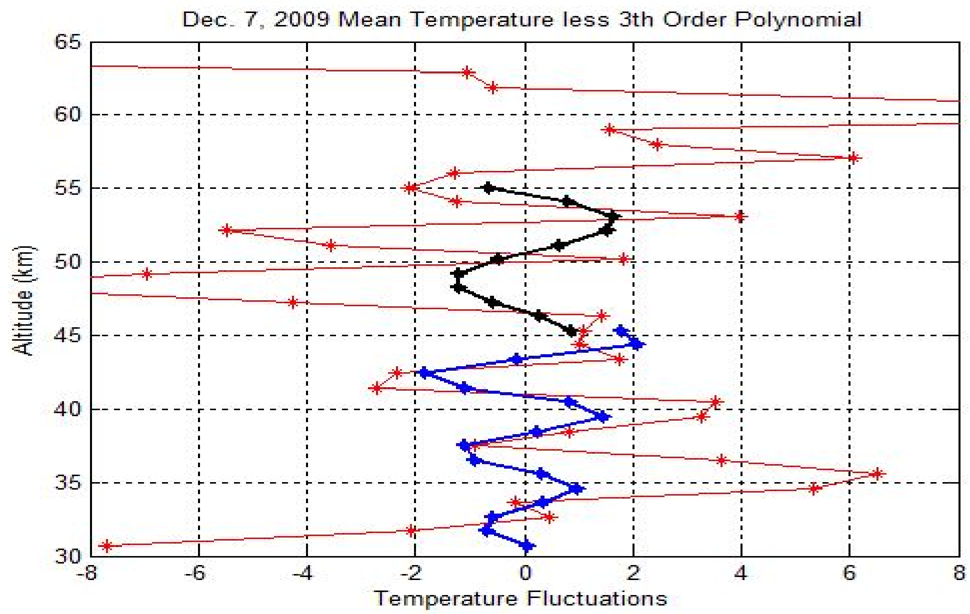

Figure 50: Vertical Fluctuations Fit for December 7, 2009

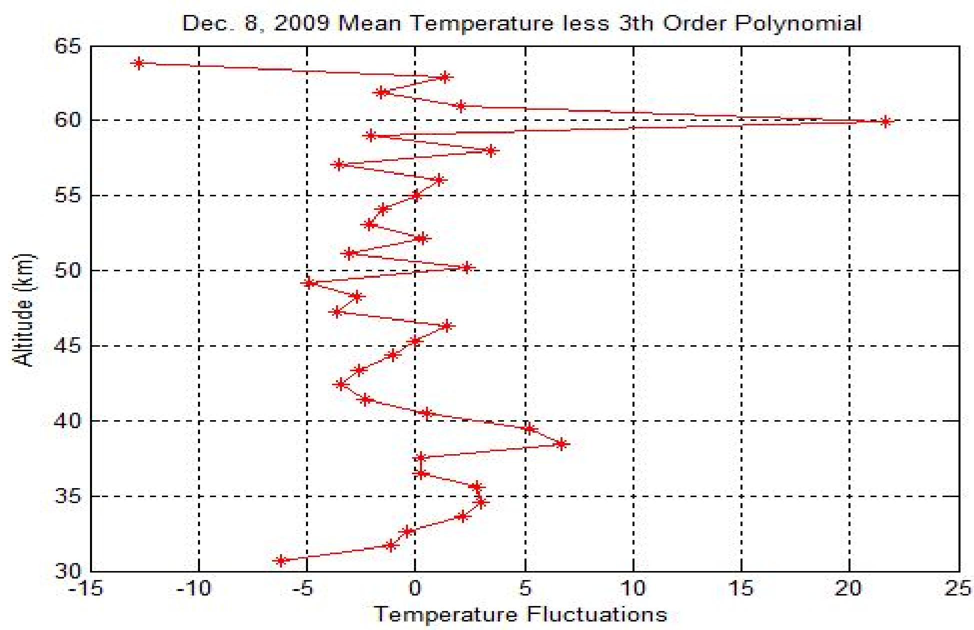

Figure 51: Vertical Fluctuations for December 8, 2009

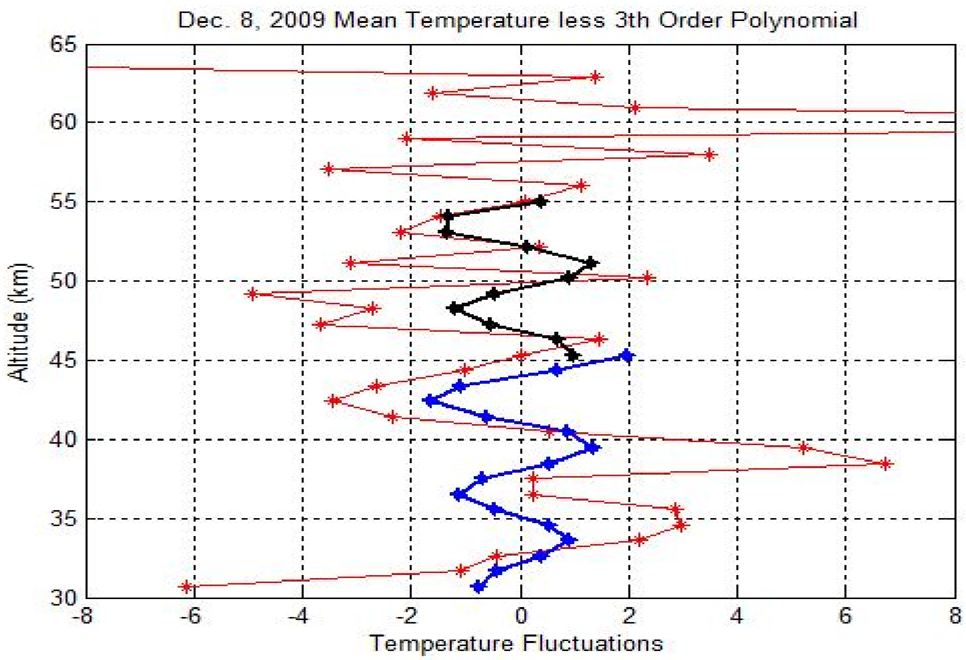

Figure 52: Vertical Fluctuations Fit for December 8, 2009

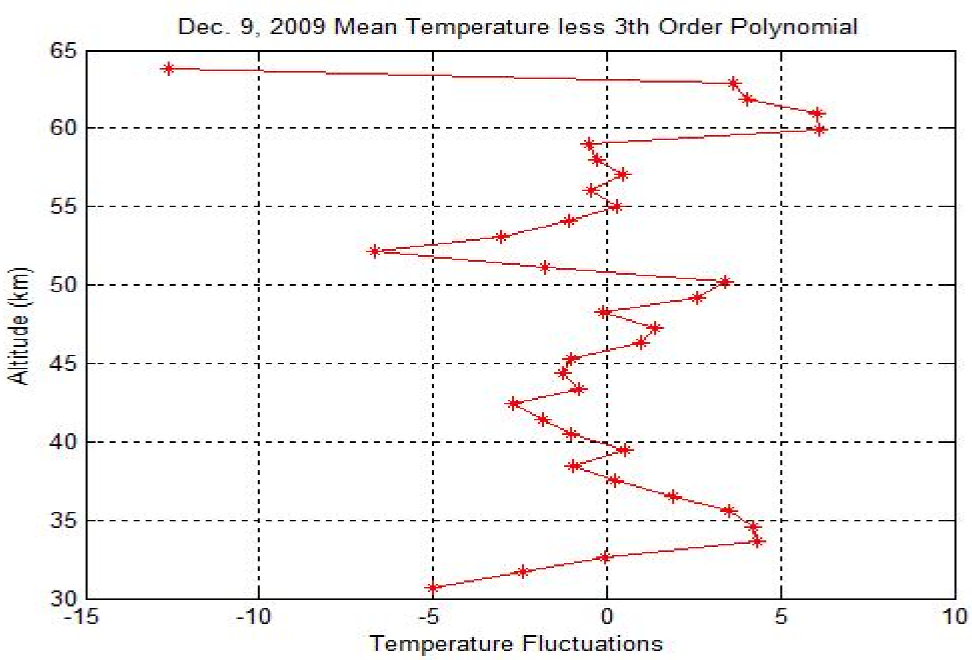

Figure 53: Vertical Fluctuations for December 9, 2009

3.5.3 Gravity Waves Detection

In a recently work, gravity waves were identified from 30 to 70 km [Deepa et al., 2006]. Spectral analysis using Fourier techniques were used in order to detect periodicities. A spectral analysis and its applications are explained by Jenkins [Jenkins et al., 1968]. Brentha et al. present another recommendation for the observation of gravity waves [Brentha et al., 2010]. They recommend the use of relative density fluctuations to characterize wave activity. They conclude that the temperature fluctuations add bias to the analysis, unlike working with the relative density fluctuations.

Carmen J. Nappo presented a description the gravity waves [Nappo, 2002]. In addition, James R. Holton offered thorough theoretical review of gravity waves in his book [Holton, 1992].

Molinaro presents another approach to vertical wavelength and height analysis in order to explain general stratospheric circulation variations of the Brunt frequency and temperature gradients [Molinaro et al., 1996]. This is an attempt to understand the dynamics of the middle atmosphere through Lidar sounding techniques and a few case studies showing local variability.

Figure 54 presents an example of the periodogram obtained by our code. See APPENDIX A.

Feb. 17, 2002 Regular Method

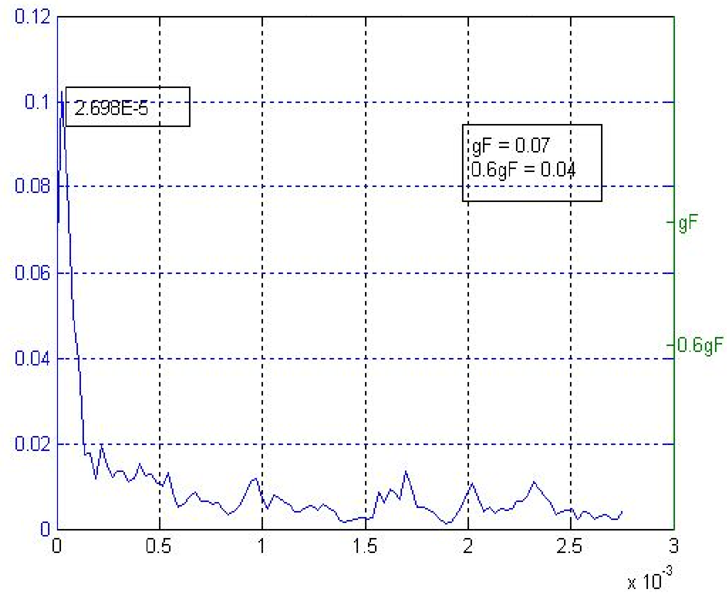

Figure 54: Periodogram with Fourier analysis
(Significant frequency = 2.698E-5 Hz)

When we talk about gravity waves it is correct to obtain a characterization of the dynamic in the lower atmosphere. Figure 55 and Figure 56 show a sample for December 7, 2009, of the zonal and meridional winds below 30km altitude. We can obtain wind observations for the previous and subsequent days of the campaign.

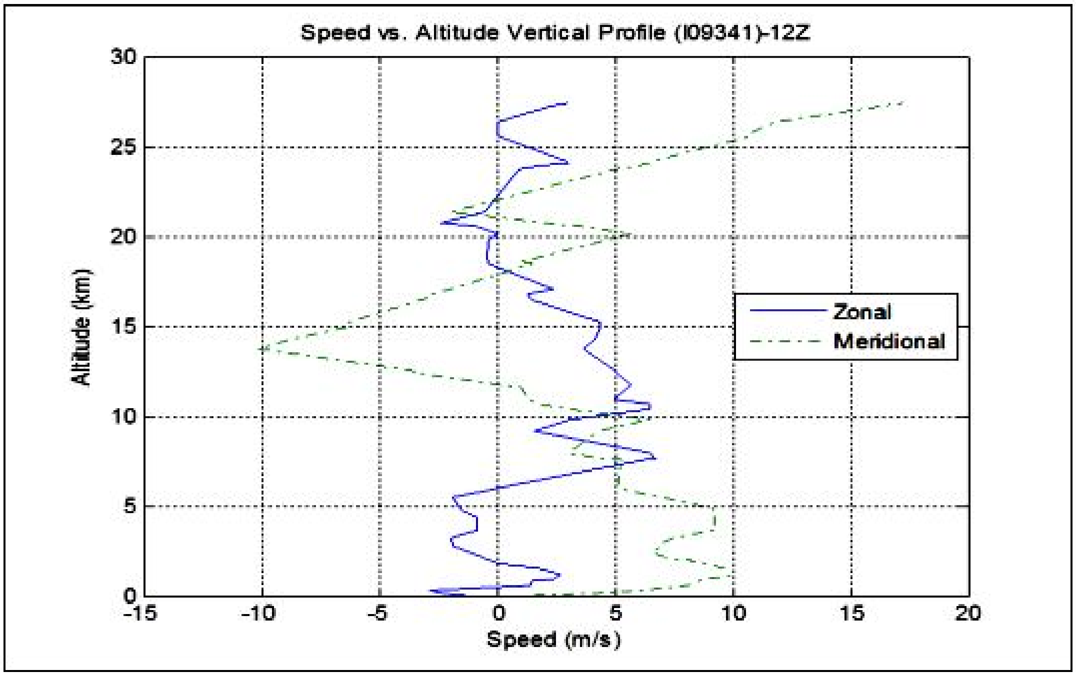

Figure 55: Zonal and Meridional Winds 12Z

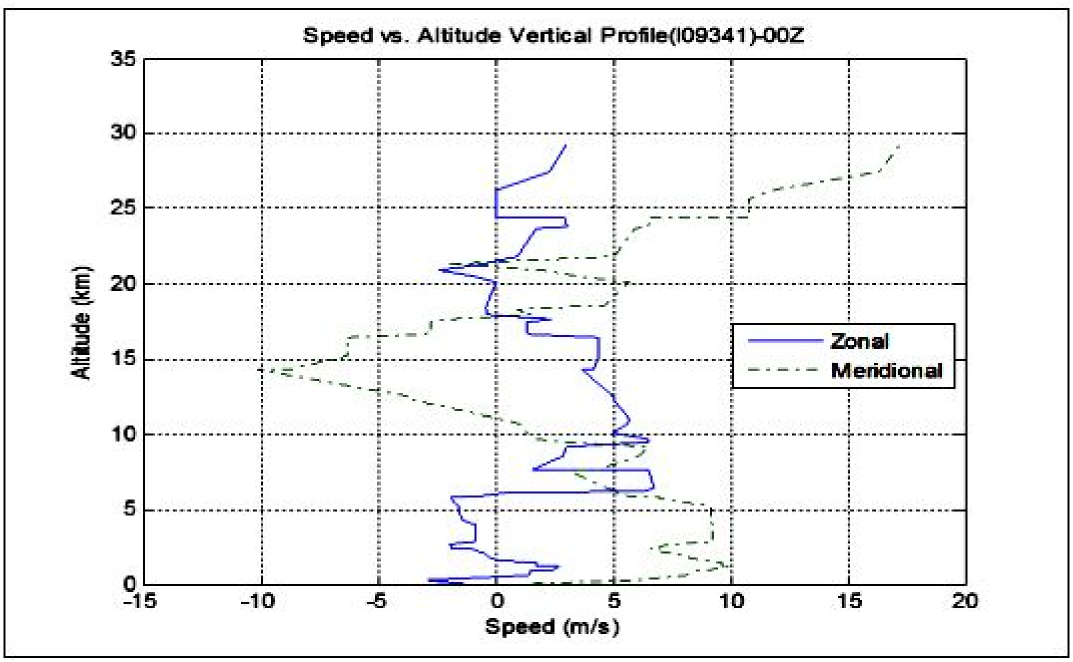

Figure 56: Zonal and Meridional Winds 00Z

3.5.4 Spectral Analysis for Evenly and Unevenly Sample Data

A Lomb and Scargle technique is used instead of conventional Fourier methods for the spectral analysis of the unevenly sampled data. Scargle modified the standard periodogram formula, rather than just taking dot products of the data with sine and cosine waveforms directly. It is necessary to first find a time delay τ such that a pair of sinusoids would be mutually orthogonal at sample time t_j, and also adjusted for the potentially unequal powers of these two basis functions, to obtain a better estimate of the power at a frequency [Press, 2007]. This process made his modified periodogram method exactly equivalent to Lomb's least-squares method. The time delay τ is defined by the formula:

$$\tan 2\omega\tau = \frac{\sum_j \sin 2\omega t_j}{\sum_j \cos 2\omega t_j}. \tag{3.1}$$

The periodogram at the frequency ω estimated as:

$$P_x(\omega) = \frac{1}{2}\left(\frac{\left[\sum_j X_j \cos\omega\left(t_j - \tau\right)\right]^2}{\sum_j \cos^2 \omega\left(t_j - \tau\right)} + \frac{\left[\sum_j X_j \sin\omega\left(t_j - \tau\right)\right]^2}{\sum_j \sin^2 \omega\left(t_j - \tau\right)} \right), \tag{3.2}$$

which Scargle reports has the same statistical distribution as the periodogram in the evenly-sampled case [Scargle, 1982]. At any individual frequency ω, this method gives the same power as does a least-square fit to sinusoids of that frequency, of the form:

$$\phi(t) \approx A\sin\omega t + B\cos\omega t. \tag{3.3}$$

Figure 57 presents a periodogram using the *Lombscargle* method. See Appendix A. In this work, the code for processing the unevenly spaced data provided by the AO staff was not evaluted. We only ran the code, and obtained results. A revision is needed for future work.

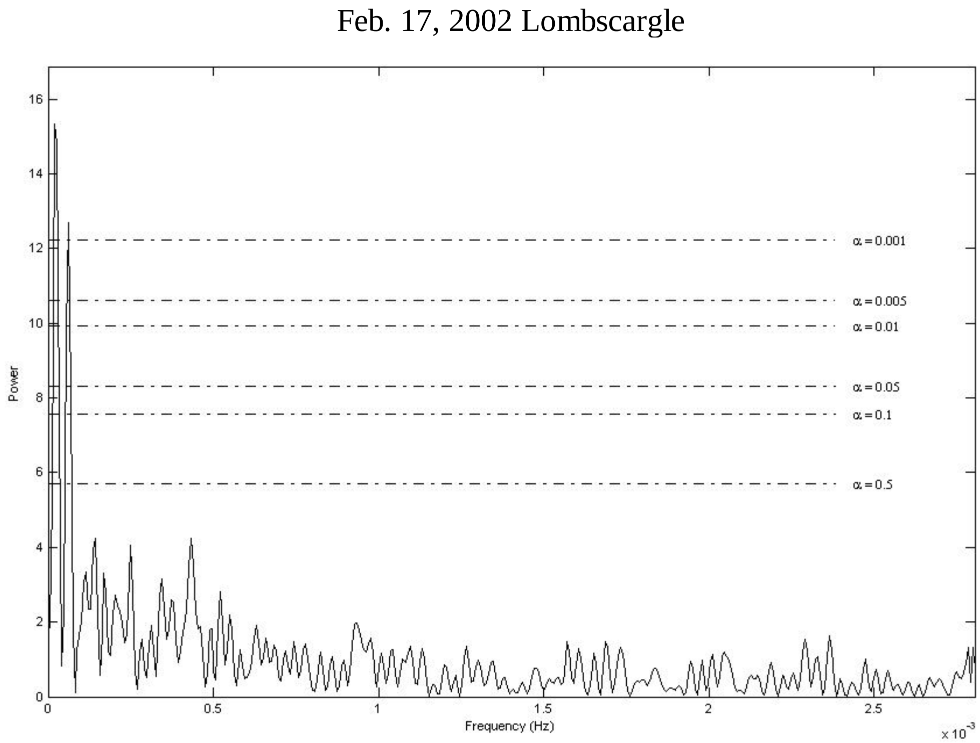

Figure 57: Periodogram by Lombscargle Method
(Significant freq. = 2.03E-5 Hz, 6.10E-5 Hz)

3.5.5 Interpretation Techniques using Fisher Test and Siegel Test

A probability test called the Fisher Test is used to verify that a power peak in the spectral analysis has a high confidence percentage of being a signal [Chun et al., 2006]. The idea is to use a probability detection method to help determine if a spectral peak is significant or not. The limits are between white noise and the spectral lines plus white noise.

Excluding the zero and Nyquist frequencies, the test is supported by the fact that under the null hypothesis that $\{X_t\}$ is a Gaussian white noise, the calculated periodogram ordinates at the Fourier frequencies are distributed as independent and identically distributed χ_2^2 rv's times a multiplicative constant. Then the test is referenced for periodogram ordinates of a size incompatible with the null hypothesis. It is assumed that any spectral lines occur at Fourier frequencies.

For mathematical convenience, the length of the realization N is odd. We can define $\left\lfloor \frac{N}{2} \right\rfloor = m$ for some positive integer m in N = 2m + 1. The periodogram terms are rescaled as:

$$\tilde{S}(f_k) \equiv \frac{\hat{S}(f_k)}{\sum_{j=1}^{m} \hat{S}(f_j)}, \tag{3.4}$$

using a Siegel (1980) suggestion for compound frequencies, even though our temperature time series are nearly monochromatic, as mentioned in Section 1.1.

We can consider g as the maximum of the sum of squares due to a single frequency f_k over the total sum of squares. Increasing m, will improve the approximation for Fisher's test. We can find α , the level of the test, equal to 0.01, 0.02, 0.05, and 0.1. The approximation of Fisher's test is:

$$g_F \approx 1 - \left(\frac{\alpha}{m}\right)^{\frac{1}{(m-1)}}. \tag{3.5}$$

Using $\lambda = 0.6$, we can calculate the statistic in Siegel's test as:

$$T_{\lambda} \equiv \sum_{k=1}^{m} \left(\tilde{S}(f_k) - \lambda \cdot g_F \right)_{+} \quad (3.6)$$

Where $(a)_+ = \max(a,0)$. For α equal to 0.05 and 0.01, we have the interpolations formula for values of m respectively as:

$$t_{0.6} = 1.0330 \cdot m^{-0.72356} \quad (3.7)$$

$$t_{0.6} = 1.4987 \cdot m^{-0.79695} \quad (3.8)$$

3.5.6 Results

By a recommendation of the Optical Science Group of the Arecibo Observatory, a *sgolayfilt* MatLab function was used to smooth the data. Then we subtracted the mean, and applied the *lombscargle* code (APENDIX A). I ran this code for the three days of the 2002 campaign. We recommend analyzing this code for future work to make comparisons with our code. Tables 3 and 4 present the obtained frequency results. Table 3 shows results for the unevenly spaced data analysis. Table 4 shows results for the conventional FFT analysis. I observed multiple significant frequencies at various altitudes. It is known that for the middle atmosphere the waves are composed of a singular frequency. We wanted to smooth the frequency background noise by using the DPSS window in our work in order to remove the long-term trend.

Table 3: Significant Frequencies

	R2002046	R2002047	R2002048
Altitude (km)	Significant Frequencies (Hz)	Significant Frequencies (Hz)	Significant Frequencies (Hz)
30.9	1.46E-05	1.80E-05	6.80E-06 4.74E-05
31.9	1.46E-05	8.99E-06	2.03E-05 5.42E-05
33	1.46E-05	1.80E-05 6.30E-05	1.40E-05 5.42E-05
34	1.46E-05 2.19E-05	8.99E-06 6.30E-05	6.80E-06 5.42E-05
35.1	2.19E-05	8.99E-06 6.30E-05	3-frequencies
36.1	1.46E-05	8.99E-06 6.30E-05	4-frequencies
37.2	1.46E-05	1.80E-05	3-frequencies
38.2	2.19E-05	8.99E-06	3-frequencies
39.3	2.19E-05	8.99E-06	2.71E-05
40.3	2.92E-05	2.70E-05	2.03E-05 6.10E-05
41.4	4.38E-05	3.60E-05	2.03E-05 5.42E-05
42.4	5.85E-05	3.60E-05	2.03E-05
43.5	5.85E-05	3.60E-05	N/A
44.5	6.58E-05	3.60E-05	N/A
45.6	2.92E-05	3.60E-05	N/A
46.6	2.92E-05	3.60E-05	N/A
47.7	2.92E-05	2.70E-05	N/A
48.7	2.92E-05	2.70E-05	N/A
49.8	2.92E-05	2.70E-05	N/A
50.8	N/A	2.70E-05	N/A
51.9	N/A	3.60E-05	N/A
52.9	N/A	2.70E-05	2.71E-05
54	N/A	2.70E-05	N/A
55	N/A	2.70E-05	N/A
56.1	N/A	1.80E-05	N/A
57.1	N/A	8.99E-06	N/A
58.2	3.65E-05	1.80E-05	N/A
59.2	3.65E-05	2.70E-05	N/A
60.3		N/A	2.71E-05
61.3		7.20E-05	2.71E-05
62.4		N/A	N/A
63.4		2.70E-05	5.42E-05
64.5		2.70E-05	N/A
65.5		2.70E-05	N/A
66.6		2.70E-05	N/A
67.6		8.99E-06	5.42E-05
68.7		1.80E-05	N/A

69.7	N/A	2.70E-05	2.71E-05
70.8	N/A	2.70E-05	2.71E-05
71.8	N/A	N/A	
72.9	N/A	N/A	
73.9	1.34E-03	N/A	

The data are unevenly spaced and we need a continuous sampling to run the conventional Fourier analysis. I decided to fill the gaps in the data using an interpolation over the gaps. Then, I could apply our conventional analysis and compare it with the *lombscargle* analysis. Below in Table 4, we show significant frequencies for the February 18, 2002. For example, we can observe that at 52.9 km, the frequency in both methods is approximately equal. For *lombscargle* is 2.71E-05, and for the FFT is 2.698E-05. No considerable propagation of waves was detected for the two campaigns by the frequency analysis, except for these periods of approximately ten hours that are not consistent by several altitudes. Sivakumar et al. (2006) indicate that vertical wavelengths greater than approximately 4 – 5 km correspond to longer periods waves (> 4.5 hours). We observe in Figure 50 and Figure 52 a vertical wavelength of approximately 4 km. We suspect that this vertical wavelength is the result of a low propagating wave knowing as an internal gravity wave. Due to the short length of observation, we cannot observe the phenomena in the frequency analysis.

Table 4: Significant Frequencies

	R2002048
Altitude (km)	Significant Frequencies (Hz)
30.9	2.70E-05
31.9	2.70E-05
33	2.70E-05
34	2.70E-05
35.1	2.70E-05
36.1	2.70E-05
37.2	2.70E-05
38.2	2.70E-05
39.3	2.70E-05
40.3	2.70E-05
41.4	2.70E-05
42.4	2.70E-05
43.5	N/A
44.5	N/A
45.6	N/A
46.6	N/A
47.7	N/A
48.7	N/A
49.8	N/A
50.8	2.70E-05
51.9	2.70E-05
52.9	2.70E-05
54	2.70E-05
55	2.70E-05
56.1	5.40E-05
57.1	N/A
58.2	N/A
59.2	N/A
60.3	2.698E-05
61.3	2.698E-05
62.4	5.395E-05
63.4	N/A
64.5	N/A
65.5	N/A
66.6	N/A
67.6	N/A
68.7	N/A
69.7	2.70E-05
70.8	2.70E-05

71.8	
72.9	
73.9	

4 Summary, Conclusions and Future Work

Processing analysis techniques were implemented to prepare the data and to apply a frequency analysis to search for periodicities in the middle atmosphere over Arecibo using Lidar observations. The algorithms obtained information for vertical and time profiles of temperature measurements. The Lidar data were compared with the standard MSIS-90 model. Vertical temperature profiles presented good fit from 35 to 48 km, approximately for the 2009 campaign. Below 35 km the temperatures is higher for this campaign. Above 48 km a bias is clearly observed from the standard model. For the 2002 campaign, the experimental temperature profile looks higher above approximately 45 km and looks lower below 45 km.

The wavelengths used for the observations were 355 nm and 532 nm. We observed by statistical analysis that the second wavelength introduced less noise to the observations, and reasonable data was obtained from higher altitudes. The pre-processing analysis permitted us to observe if the data was evenly or unevenly sampled. The 2002 campaign was analyzed using short periods of observations due to the time gaps. After developing an algorithm for frequency analysis we were able to search for waves using a periodogram. On December 7 – 8, 2009, we observed a wave with a vertical wavelength of approximately 4 km. We suspect that this vertical wavelength is the result of a low propagating wave known as an internal gravity wave. Due to the short length of observations, we cannot observe the phenomena in the frequency analysis. We can, however, validate our suspicion because we do not observe strong phase propagation in the time sequence for the vertical temperature profiles. We recommend taking more Lidar observations in different seasons, in order to better study the wave morphology of the region.

APPENDIX A: Codes in MatLab

- **timeseries.m**

This code plots a figure that presents a set of five desired altitudes for the temperature time series fluctuations. The code identifies the anomalous increments and reflects the gaps in the time series.

- **timeincrement.m**

This code evaluates the time increments of the sampling data. It determines the numerical value of the anomalous increments and their position in time.

- **Bi_dimensional.m**

This program presents a bi-dimensional representation of the data. It presents a time versus altitude representation for a matrix of temperatures. The code provides the option to present fluctuations, instead of temperature, by subtracting the mean at each altitude.

- **nan_bi_dimensional.m**

This code generates a matrix of NaN (not a number) values present in the data.

- **verticalprofile.m**

This code generates a figure that illustrates the mean vertical temperature profile, using the MSIS-90 model for adesired day. A third order polynomial fit is also plotted.

- **verticalprofilebyparts.m**

This application provides an average of the vertical temperature profile in four intervals.

- **histograms.m**

The data distribution by altitude is presented using histograms. The code includes a function to present a probability plot, which facilitates the visualization of outliers.

- **brunvaisalafreq.m**

This code generates a graph of the Brunt Vaisala frequency.

- **provesgolayfilt.m**

This code verifies the *sgolay.m* function, which is a filter, used to smooth the data before applying spectral analysis.

- **lombscargle.m**

This code implements the spectral analysis for unevenly spaced data. Dr. Sumanta Zarkhel, member of the Optical Science Group at the Arecibo Observatory, provided this code.

APPENDIX B: **VITMO Model - Web Browser Results for MSIS-90 Model listing for February/2002**

Intut parameters

year= 2002, month= 02, day= 15, 16, 17, hour=20.,
Time_type = Local
Coordinate_type = Geographic
latitude= 18., longitude= 66., height= 100.
Prof. parameters: start= 30.863 stop= 73.912 step= 1.05

Table 5: MSIS-90 Model Listing for Feb./2002

	2/15/2002		2/16/2002		2/17/2002	
1	2	3	2	3	2	3
30.9	1.586E-05	229.0	1.586E-05	229.0	1.587E-05	229.0
31.9	1.343E-05	232.0	1.343E-05	232.0	1.343E-05	232.0
33.0	1.137E-05	235.5	1.137E-05	235.5	1.137E-05	235.5
34.0	9.644E-06	239.1	9.644E-06	239.1	9.645E-06	239.1
35.1	8.203E-06	242.6	8.203E-06	242.7	8.204E-06	242.7
36.1	6.996E-06	246.2	6.996E-06	246.2	6.996E-06	246.2
37.2	5.982E-06	249.6	5.982E-06	249.6	5.982E-06	249.7
38.2	5.129E-06	252.9	5.129E-06	252.9	5.129E-06	253.0
39.3	4.410E-06	256.0	4.410E-06	256.1	4.410E-06	256.1
40.3	3.802E-06	258.9	3.802E-06	259.0	3.801E-06	259.0
41.4	3.286E-06	261.5	3.286E-06	261.6	3.286E-06	261.6
42.4	2.848E-06	263.7	2.848E-06	263.8	2.848E-06	263.9
43.5	2.475E-06	265.6	2.475E-06	265.7	2.475E-06	265.8
44.5	2.157E-06	267.0	2.157E-06	267.1	2.157E-06	267.2
45.6	1.884E-06	268.0	1.884E-06	268.1	1.884E-06	268.1
46.6	1.649E-06	268.4	1.649E-06	268.5	1.649E-06	268.6
47.7	1.446E-06	268.3	1.446E-06	268.4	1.447E-06	268.5
48.7	1.270E-06	267.9	1.271E-06	267.9	1.271E-06	268.0
49.8	1.117E-06	267.0	1.118E-06	267.0	1.118E-06	267.1
50.8	9.837E-07	265.7	9.840E-07	265.8	9.844E-07	265.8
51.9	8.664E-07	264.1	8.668E-07	264.2	8.672E-07	264.2
52.9	7.634E-07	262.2	7.638E-07	262.3	7.642E-07	262.3
54.0	6.726E-07	260.1	6.730E-07	260.1	6.735E-07	260.1
55.0	5.925E-07	257.8	5.929E-07	257.8	5.933E-07	257.8
56.1	5.217E-07	255.3	5.220E-07	255.3	5.224E-07	255.3
57.1	4.589E-07	252.7	4.593E-07	252.7	4.596E-07	252.6
58.2	4.034E-07	250.0	4.037E-07	250.0	4.040E-07	249.9
59.2	3.541E-07	247.3	3.544E-07	247.2	3.547E-07	247.2
60.3	3.105E-07	244.5	3.107E-07	244.4	3.110E-07	244.4
61.3	2.718E-07	241.8	2.720E-07	241.7	2.722E-07	241.6
62.4	2.375E-07	239.1	2.377E-07	239.0	2.379E-07	238.9
63.4	2.072E-07	236.4	2.074E-07	236.3	2.075E-07	236.2
64.5	1.804E-07	233.9	1.806E-07	233.8	1.807E-07	233.7
65.5	1.568E-07	231.4	1.569E-07	231.3	1.571E-07	231.2
66.6	1.360E-07	229.1	1.361E-07	229.0	1.362E-07	228.9
67.6	1.178E-07	226.9	1.178E-07	226.8	1.179E-07	226.7
68.7	1.018E-07	224.9	1.018E-07	224.8	1.019E-07	224.6
69.7	8.774E-08	223.1	8.778E-08	222.9	8.783E-08	222.8
70.8	7.550E-08	221.4	7.554E-08	221.3	7.558E-08	221.1
71.8	6.485E-08	220.0	6.488E-08	219.8	6.490E-08	219.7
72.9	5.554E-08	218.7	5.556E-08	218.6	5.558E-08	218.4

APPENDIX C: VITMO Model - Web Browser Results for MSIS-90 Model listing for December/2009

Intut parameters

year= 2009, month= 12, day= 7, 8, 9, hour=20.,
Time_type = Local
Coordinate_type = Geographic
latitude= 18., longitude= 66., height= 100.
Prof. parameters: start= 30.6940 stop= 63.8440 step= 0.975

Optional parametes: F10.7(daily) =not specifyed; F10.7(3-month avg) =not specifyed; ap(daily) = not specifyed

```
   Selected parameters are:
1 Height, km
2 Mass_density, g/cm-3
3 Temperature_neutral, K
```

Table 6: MSIS-90 Model Listing for Dec./2009

	12/7/2009		12/8/2009		12/9/2009	
1	2	3	2	3	2	3
30.7	1.619E-05	231.8	1.619E-05	231.7	1.618E-05	231.7
31.7	1.390E-05	234.5	1.389E-05	234.4	1.389E-05	234.4
32.6	1.194E-05	237.5	1.193E-05	237.4	1.193E-05	237.4
33.6	1.027E-05	240.5	1.027E-05	240.5	1.026E-05	240.5
34.6	8.855E-06	243.5	8.852E-06	243.5	8.851E-06	243.5
35.6	7.653E-06	246.4	7.650E-06	246.4	7.648E-06	246.4
36.5	6.628E-06	249.2	6.626E-06	249.2	6.624E-06	249.1
37.5	5.753E-06	251.9	5.751E-06	251.8	5.749E-06	251.8
38.5	5.004E-06	254.3	5.002E-06	254.3	5.000E-06	254.3
39.5	4.361E-06	256.6	4.359E-06	256.6	4.358E-06	256.6
40.4	3.809E-06	258.7	3.807E-06	258.7	3.806E-06	258.7
41.4	3.333E-06	260.6	3.331E-06	260.6	3.330E-06	260.5
42.4	2.922E-06	262.2	2.920E-06	262.2	2.919E-06	262.2
43.4	2.566E-06	263.6	2.565E-06	263.6	2.564E-06	263.5
44.3	2.258E-06	264.7	2.256E-06	264.6	2.255E-06	264.6
45.3	1.989E-06	265.4	1.988E-06	265.4	1.988E-06	265.3
46.3	1.756E-06	265.9	1.755E-06	265.8	1.754E-06	265.8
47.3	1.552E-06	266.0	1.551E-06	265.9	1.550E-06	265.9
48.2	1.373E-06	265.8	1.372E-06	265.8	1.371E-06	265.7
49.2	1.216E-06	265.3	1.215E-06	265.3	1.215E-06	265.3
50.2	1.078E-06	264.6	1.077E-06	264.6	1.076E-06	264.5
51.2	9.560E-07	263.6	9.553E-07	263.6	9.547E-07	263.6
52.1	8.482E-07	262.3	8.476E-07	262.3	8.471E-07	262.3
53.1	7.529E-07	260.8	7.523E-07	260.9	7.518E-07	260.9
54.1	6.683E-07	259.2	6.678E-07	259.2	6.673E-07	259.2
55.1	5.932E-07	257.3	5.927E-07	257.3	5.923E-07	257.3
56.0	5.264E-07	255.3	5.260E-07	255.3	5.256E-07	255.3
57.0	4.669E-07	253.1	4.665E-07	253.1	4.662E-07	253.2
58.0	4.139E-07	250.8	4.136E-07	250.9	4.133E-07	250.9
59.0	3.667E-07	248.5	3.664E-07	248.5	3.661E-07	248.6
59.9	3.245E-07	246.1	3.242E-07	246.2	3.240E-07	246.2
60.9	2.868E-07	243.7	2.866E-07	243.8	2.864E-07	243.8
61.9	2.533E-07	241.3	2.531E-07	241.4	2.529E-07	241.4
62.9	2.233E-07	239.0	2.231E-07	239.0	2.230E-07	239.1
63.8	1.966E-07	236.6	1.965E-07	236.7	1.963E-07	236.8

References

Bores, C., "*FFT window functions*", Bores, S., Bores Signal Processing, Fordwater, Pond Road, Working, Surrey GU22 0JZ UK , Web: March 2, 2012, (http://www.bores.com/courses/advanced/windows/files/windows.pdf)

Chane-Ming, F., Molinaro, F., Leveau J., *"Wavelet techniques applied to Lidar temperature profiles in the Middle Atmosphere to study gravity waves"*, IEEE Trans. Geosci. Remote Sens., vol. 1, pp. 581-583, 1997 .

Chun L, A., Law, N. F., Cao, X. Q., Yang, H. S. L., C. S. Ruf and S. J. Keihm, "*Statistical power of Fisher test for the detection of short periodic gene expression profiles*", School of Information & Communication Technology, Gold Coast Campus, Griffith University, Australia, 2006.

Deepa, V., Ramkumar, G., Murthy ,V.K., *"Gravity waves obserbed from the Equatorial Wave Studies (EWS) campaign during 1999 and 2000 and their role in the generation of stratospheric semiannual oscillations"*, Annale Geophysicae, vol. 24 pp. 2481-2491, 2006

Devie, M., Barbara, A. K., "*Middle atmospheric dynamic through Lidar soundings: A few cases studies*", Department of physics, Gauhati University Guwahati-781 014, Assam, India., IEEE Trans. Geosci. Remote Sens., vol. 2, pp. 451-453, 2002

Fritts, D. C., Alexander, M. J., "*Gravity waves dynamics and effects in the middle atmosphere"*, Colorado Research Associates, Reviews of Geophysics 41 (1) 1003, 2003.

Fritts, D. C., *"Gravity wave saturation in the middle atmosphere: A review of theory and observations"*, Rev. Geophys., 22, pp 275-308, 1984

Gurahay, A., Taori, A., Taylor, M., *"Summer-time nocturnal wave characteristics in mesospheric OH and O_2 airglow emissions"*, Earth Planet Space, 60, 973-979, 2008

Hanselman, D. and Littlefield, B., "*Mastering MatLab 7"*, Pearson, Prentice Hall, Upper Saddle River, NJ, 2005

Hauchercorne, A., Chanin, M-L, *"Density and temperatures profiles obtained by Lidar between 35 and 70 km"*, Geophysical Research Letters, vol. 7, no. 8, pp. 565-568, 1980

Hines, C.O., *"Internal atmospheric gravity waves at ionospheric heights"*, Can. J. Phys., 38, 1441-1481, 1960

Holton, J. R., C., "*An Introduction to Dynamic Meteorology"*, Third edition, International geophysics series vol.48, 1992.

Hui, M., Alan, *"Layers of Atmosphere"*, Web: March 2, 2012, (http://www.vtaide.com/png/atmosphere.htm)

Lastovicka, J., Krizan, P. , and Kozubek M., *"Long-term trends in the middle atmosphere dynamics at northern middle latitudes – one regime or two different regimes?"*, Atmospheric Chemistry and Physics Discussions, 10, 2636-2668, 2010

Mackenzie, F. T., "*Our Changing Planet – An Introduction to Earth System Science and Global Environmental Change"*, Second edition, Prentice Hall, Upper Saddle River, NJ, 1998

Measure, R. M., *"Laser Remote Sensing, Fundamentals and Applications"*, Krieger Publications, Malabar, F.L., 1992

Miller, M. S., Gardner, C.S., Liu, C.H., "*Rayleigh Lidar observations of gravity wave activity in the Stratosphere and Lower Mesosphere"*, National Science Foundation Air Force Geophysics Laboratory, National Aeronautics & Space Administration, 1987

Molinaro, F., Bencherif, H., Bessafi, M., Leveau, J., "*Time-Frequency Analisys of Backscattered Lidar Signal to Study Atmosphere Dynamics*", Laboratoire de Physique de I'AtmosphCre, Universitt de la Reunion, 15 AV. Rent Cassin, BP 7151, 9771.5 Saint Denis cedex 9, France, 1996

Percival, D, Walden, A., *Spectral Analysis for Physical Applications.* Cambridge: Cambridge University Press, 1993.

Press, W., Teukolsky, S., Vetterling, W., Flannery, B., "*Numerical Recipes: The Art of Scientific Computing"* 3rd. Ed., Cambridge University Press, 2007.

Qian S. and Chen, D., *Joint Time – Frequency Analysis Methods and Applications*, Prentice Hall, Inc., Upper Saddle, NJ, 1996

Scargle, J. D., *"Studies in astronomical time series analysis. II - Statistical aspects of spectral analysis of unevenly spaced data"*, Astrophysical Journal, 263: 835, 1982.

Sivakumar, V., Rao, P.B., Bencherif, H., "*Lidar observations of the middle atmosphere gravity wave activity over a low latitude site (Gadanki, 13.5_ N, 79.2_ E)"*, Annales Geophysicae, 24, 823-834, 2006

Strauch, R., Frisch, S., Weber, B., "*Wind measurements in the upper troposphere with UHF and VHF Radar"*, American Meteorological Society, NOAA/ERL/Wave Propagation Laboratorie, 1986.

Thomas, L., Worthington, R. M., Mc Donald, A.J., "*Inertia gravity waves in the troposphere and lower stratosphere associate with a jet stream exit region*", Annales Geophysicae, 17, 115 -121 , 1999.

Thurairajah, B., Collins, R., Harvey V. L., Lieberman, R. S., Mizutani, K., "*Rayleigh Lidar observations of reduced gravity wave activity during the formation of an elevated stratopause in 2004 at Chatanika, Alaska (65° N, 147° W)*", Journal of Geophysical Research, vol. 115, D13109, pp. 1-14, 2010

Weitkamp, C., "*Lidar: Range-Resolved Optical Remote Sensing of the Atmosphere*", Springer Science & Business Media, Inc., 2005

West, F., "*MF Radar study of the middl atmosphere and development of visualization and spectral analysis software*", University of P.R. at Mayaguez, Thesis, 1999